Materials Advances

ROYAL SOCIETY OF CHEMISTRY

REVIEW

View Article Online
View Journal | View Issue

Cite this: *Mater. Adv.*, 2024, 5, 896

Rational design of SiO_x based anode materials for next generation lithium-ion batteries

Yuanteng Yang,[a] Yanxia Liu,[a] Xiaoli Jiang,[a] Lin Zhao,[a] Penglei Wang *[b] and Yagang Zhang *[a]

Lithium-ion batteries (LIBs) have gained significant importance in various fields, as they play a vital role in energy storage and conversion. The design and development of anode materials are of the utmost significance in enhancing the electrochemical performance of LIBs. SiO_x has emerged as a promising candidate for the next generation of anode materials, primarily due to its high energy density, which has garnered widespread attention. However, the commercialization of SiO_x has been hindered by challenges such as low conductivity and significant volume change during cycling. The design of SiO_x/C composites offers a potential solution to circumvent most of the inherent drawbacks of SiO_x, as carbon materials possess excellent electrochemical and physical properties. In this review, we aim to provide an in-depth analysis of SiO_x with different dimensions, with a specific focus on the influence of the oxidation degree on the electrochemical performance. We classify the recent representative progress in SiO_x/C composites based on their structural characteristics and highlight the structure–activity relationship of different materials. Additionally, strategies for improving the performance of SiO_x based anode materials are discussed, including the use of carbon sources, doping, surface modification, prelithiation and the use of binders. Finally, the challenges and research prospects are also described, aiming to provide insights for the rational design of advanced SiO_x/C composites.

Received 15th October 2023,
Accepted 4th December 2023

DOI: 10.1039/d3ma00859b

rsc.li/materials-advances

1. Introduction

In light of the depletion of fossil fuels and the challenges posed by climate change, there is a pressing need to develop green energy solutions to alleviate the energy crisis. Lithium-ion batteries (LIBs) have been comprehensively improved and are widely used in various fields due to their higher specific capacity and longer cycle life compared to traditional batteries.[1,2] The widespread interest and utilization of LIBs in diverse electronic devices, along with their integration with renewable energy sources like wind and tidal power, have led to a surge in practical applications.[3,4] The specific capacity is one of the most important indicators for evaluating LIBs. Research indicates that the capacity of LIBs is consistently advancing at a rate of 7% to 10% per year. This highlights the crucial importance of continuous innovation in battery technology to meet the ever-increasing demand for energy storage solutions.[5] LIBs primarily comprise an anode, a cathode, separators, and electrolytes (Fig. 1a). The anode material holds significant importance in the overall system, playing a pivotal role in determining the specific capacity of the battery (Fig. 1b).[6] In the early days of LIB development, coke was commonly used as the anode material. Most anode materials currently used in commercially available LIBs still consist of carbon materials. This choice is primarily driven by the excellent cycle performance and enhanced safety characteristics offered by carbon-based anodes.[7,8] However, the low specific capacity of graphite (372 mA h g^{-1}) has been unable to meet the demand of LIBs. In order to break through the problem of low specific capacity, it is necessary to seek the next generation of LIB anode materials.[8]

Si is considered one of the most promising next-generation anode materials for LIBs due to its high specific capacity of approximately 3400 mA h g^{-1}, which is much higher than those of carbon materials. This makes it highly attractive for use in high performance batteries that require a high energy density. In addition to its high specific capacity, Si is also abundant in nature and easy to obtain, making it an attractive option for large-scale battery production.[9] Nevertheless, one major challenge encountered with silicon as a negative electrode is its significant volume expansion (300%) during the charging/discharging process. The volume expansion makes the electrode deform and the electrode material structure collapse. At the same time, the solid–electrolyte interphase (SEI) film will also

[a] School of Materials and Energy, University of Electronic Science and Technology of China, Chengdu, 611731, Sichuan, China. E-mail: ygzhang@uestc.edu.cn, plwang@phy.cuhk.edu.hk
[b] Department of Physics, the Chinese University of Hong Kong, Shatin, Hong Kong SAR 999077, China

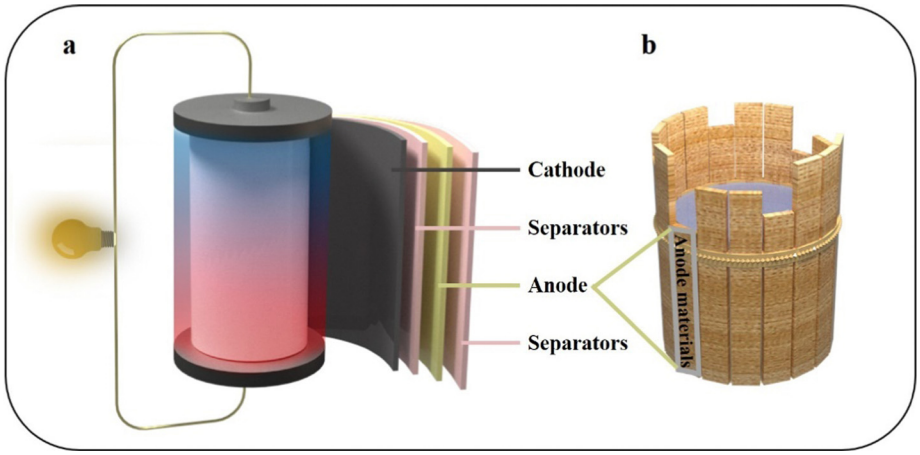

Fig. 1 Schematic diagram of (a) the LIBs structure and (b) anode materials, which play a decisive role in LIBs.

break, causing the Si to be in contact with the electrolyte, constantly generating the SEI, consuming the electrolyte, and seriously affecting the electrochemical performance. In addition, the electronic transmission capacity of Si based materials is also far less than that of graphite, which severely limits their application in LIBs.[10,11]

It is found that SiO_x is a mixture of Si and SiO_2 and some metastable silicon oxides, so the theoretical specific capacity is also between those of SiO_2 (1600 mA h g^{-1}) and Si (4200 mA h g^{-1}).[12] However, SiO_x exhibits significantly reduced volume expansion compared to pure Si, making it a promising candidate for high-performance batteries. The lithium intercalation mechanism is different due to the change of Si species.[13] An inert layer of LiO_2 and lithium silicate will be formed in the outer layer of SiO_x, which will significantly improve the stability of the SEI and ultimately improve its cycling performance.[14] Unfortunately, SiO_x still has a volume expansion of more than 160%, and the addition of oxides has significantly reduced the conductivity, which poses a challenge for its commercialization.[15] The electrochemical performance of SiO_x based anode materials can be effectively improved through reasonable material design.[16,17] The design of hollow structures offers a viable solution to address the issue of volume expansion, making it possible to mitigate this change. Additionally, the use of SiO_x/C composite anode materials is widely recognized as the most effective method to overcome this limitation. The second challenge associated with SiO_x is low conductivity.[18] Combining carbon with SiO_x in a composite material can not only mitigate volume changes, but also take advantage of the excellent chemical properties and superior conductivity of carbon, which can facilitate the transfer of both electrons and ions.[19] While there have been many reviews summarizing the research progress of Si based anode materials for LIBs, research focused on SiO_x is relatively limited.[20,21] This review aims to provide a comprehensive summary and analysis of notable research advancements in the field of SiO_x anode structural design. Specifically, it emphasizes the distinguishing features of SiO_x core structures and their profound impact on electrochemical performance. The importance of oxygen content is analysed, and the value of x should be reasonably controlled during the synthesis of SiO_x. According to the different structures of SiO_x/C composites, the synthesis methods and the structure–activity relationship are summarized. Furthermore, it highlights several optimization strategies aimed at enhancing the performance of SiO_x/C, with particular emphasis on the hybridization of diverse carbon sources with SiO_x. Lastly, this review discusses the current challenges that SiO_x/C composites still encounter, aiming to stimulate discussions and generate ideas that can contribute to the progress of SiO_x/C composites. It is hoped that this review will inspire further advancements in the field.

2. Crystal structures of SiO_x and carbon materials

SiO_x based anode materials are considered one of the most attractive alternatives to graphite because of their high specific capacity and stable voltage platform. To make better use of SiO_x, we must have a more comprehensive understanding of SiO_x.[22] In the past decades, many efforts have been made to analyse the crystal structure and energy storage mechanism of SiO_x.[23] Due to the limited characterization instruments, the early understanding of SiO_x was controversial and incomplete. Some researchers argued that SiO_x, as reported by Philipp, exists in a single-phase state, where continuous Si–Si and Si–O bonds randomly distribute within the SiO random network, forming SiO_x materials.[24,25] On the other hand, another group of researchers supported the notion that SiO_x is a two-phase mixture, with SiO_2 and Si randomly mixed together.[26] By 2003, Hohl *et al.*[27] and Fuglein *et al.*[28] characterized SiO_x by more advanced characterization methods (XPS, HRTEM, NMR, ESR, *etc.*) and proposed an interface cluster model. In Fig. 2a, the white regions may signify clusters of SiO_2, while the black regions may represent clusters of Si. Additionally, the grey regions could denote either transitional silicon oxide (SiO) or

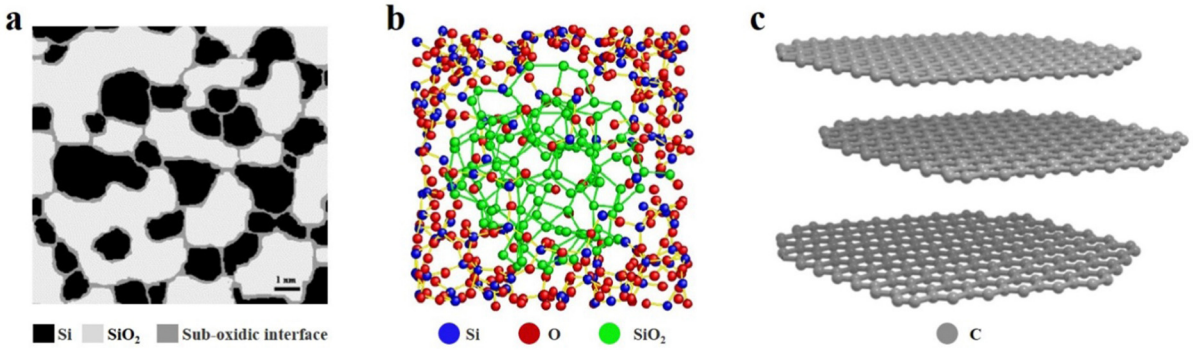

Fig. 2 (a) Schematic illustration of the interface cluster mixture structure of a-SiO. Reproduced with permission.[27] Reproduced from ref. 27 with permission from Elsevier, Copyright 2003. (b) Reconstructed heterostructure model of amorphous SiO.[29] Reproduced from ref. 29 with permission from Springer Nature, Copyright 2016. (c) Crystal structure model of graphite.

a blend of SiO_2 and Si. In the past decade, researchers have also proposed an intermediate model, according to which amorphous SiO_2 and amorphous Si exist in amorphous SiO, and the transition phase SiO_x is wrapped by the two phases (Fig. 2b).[29] The energy storage mechanism of SiO_x is similar to that of Si in the sense that both materials will generate a lithium–Si alloy (such as $Li_{13}Si_4$, Li_7Si_3, and $Li_{12}Si_7$) during the charge/discharge process in a lithium-ion battery. However, in the case of SiO_x, additional reactions occur, resulting in the formation of Li silicates (such as Li_4SiO_4, Li_2SiO_3, and Li_2SiO_5) and Li_2O. Li_2O can act as a Li^+ diffusion medium, facilitating Li^+ transport and improving the rate performance of the battery. Moreover, Li_2O and Li silicate can also buffer the volume expansion of SiO_x during cycling.[30] According to research findings, a higher oxygen content in SiO_x can lead to the formation of additional by-products such as Li silicate (Li_2SiO_3) and Li_2O during the initial charge/discharge cycles of the battery. The reaction that produces these by-products is irreversible, which will consume a large amount of Li^+ and greatly reduce the initial coulomb efficiency (ICE). The Si in SiO_x has a regular tetrahedral structure with good crystallinity, so it has strong rigidity, but weak elasticity and conductivity. With the insertion of Li^+, the change of volume will produce large stress in the electrode. If the stress exceeds the elastic range of the material, it will lead to cracking or even pulverization of the electrode material, which will seriously affect the life of the battery.[31] After 20 years of research and development, it is indeed apparent that utilizing high-capacity SiO_x-based anode materials in lithium-ion batteries (LIBs) remains a challenging task.[32]

The application of carbon materials in the anode of LIBs is well-explored, with graphite being the most commonly used and mature material. The layered structure is the unique characteristic of graphite, and the interlaced graphene layers are connected by van der Waals forces and metal bonds (Fig. 2c).[33] The force between graphene layers in graphite is weak, allowing the layers to easily slip past each other, which contributes to the excellent mechanical properties of graphite. This property is beneficial in the context of LIBs as graphite can provide a stress buffer to accommodate the volume changes that occur in the SiO_x material during cycling. By serving as a mechanical support, graphite can help to prevent the degradation and fracture of the SiO_x material, thereby improving the overall cycling stability and performance of the battery.[34] The carbon of graphite is sp^2 hybridized, and six carbon atoms form a planar hexagonal structure on the same plane. In addition, each carbon atom has a delocalized valence electron to form a big π key, and the electrons can move freely between the graphene layers. The delocalized Π electrons endow graphite with excellent electronic conductivity. Alongside graphite, the carbon materials in SiO_x/C composites include graphene, carbon nanotubes, multiwalled carbon nanotubes (MWCNTs), fullerene, *etc.*[35] These materials have desirable mechanical and electrochemical properties. For instance, the inclusion of carbon nanotubes in SiO_x can enhance conductivity by providing additional pathways for ion and electron transport.[36] Nevertheless, the practical utilization of these materials is often hindered by high production costs or complex manufacturing processes, thereby limiting their industrial-scale production.[37]

The lower specific capacity of carbon materials limits their application as anode materials when used alone. Research has shown that the combination of SiO_x and carbon materials can achieve the superposition of their advantages.[38]

3. SiO_x design

3.1. SiO_x structure design

In order to realize the potential of SiO_x/C composites as anode materials with excellent electrochemical performance, it is essential to carefully design the SiO_x precursors.[39] The size and morphology of the SiO_x core can significantly impact the electrochemical performance of the composites. It is essential for a valuable process to not only prioritize cost considerations but also place significant emphasis on environmental friendliness.[40] Some of the most common nanostructures used in SiO_x precursors include nanoparticles, porous nanoparticles, hollow nanoparticles, nanowires, and nanofilms. These structures can significantly improve the cycle stability and coulomb

efficiency of SiO_x based anode materials. By optimizing the synthesis and design of SiO_x precursors, it is possible to achieve SiO_x/C composites with excellent electrochemical performance and long-term cycling stability.[41,42]

3.1.1. SiO_x particles

3.1.1.1. 0D SiO_x particles. SiO_x particles are one of the most fundamental designs and have been intensively researched due to their manufacturing compatibility and commercial availability.[43] Miraculously, it has been shown that reducing the diameter of the SiO_x core can attenuate the volume expansion. In the process of material exploration, various experimental routes have been developed to synthesize homogeneous SiO_x nanoparticles.[44] Tao *et al.*[45] prepared a mixture of tetraethyl orthosilicate (TEOS) and citric acid under intense stirring. The mixture was polymerized with ethylene glycol through polyesterification reaction, and then the polymer gel was obtained by ultrasonic atomization. Finally, SiO_x/C was obtained by spray drying in an Ar/H_2 mixture atmosphere. Xi *et al.*[46] chose the Si particles from a chemical company and then modified the surface oxide by HCl pickling. Si particles were mixed with formaldehyde–water solution and resorcinol to form the precursors of phenolic resin coated Si/SiO_2. Subsequently, Si/SiO_x/C was obtained after high-temperature carbonization of the precursor. Similarly, Cao *et al.*[47] reported a simple and less costly method to obtain SiO_x by ball-milling Si powder in air, which can achieve simple control of oxygen content.

3.1.1.2. 3D SiO_x particles. The secondary structure adjustment of SiO_x particles can enhance their cycle performance. Porous SiO_x particles were etched on the surface to leave many channels, which can shorten the transmission distance of ions and electrons and achieve high-rate charging/discharging.[48] Kin *et al.*[49] reported an efficient strategy for preparing porous SiO_x. It involved mechanical milling of SiO_2 with zinc, and then Zn/SiO_2 was calcined at high temperature. Because the melting point and boiling point of Zn are relatively low, the redundant Zn will evaporate more easily to remove after reducing SiO_2. SiO_x with many mesopores can be obtained by this process. Zeng *et al.*[50] synthesized cauliflower like Si/SiO_x particles by incomplete magnesium thermal reduction of SiO_2. SiO_2 nanoparticles were prepared by hydrothermal reaction of TEOS, urea, pentanol and cetylpyridinium bromide. Then SiO_2 particles, Mg and NaCl were subjected to high temperature solid phase reaction at 700 °C to obtain porous CF-Si/SiO_x-700. Finally, the redundant Mg and MgO were washed away by HCl. CF-Si/SiO_x-700 was characterized by scanning electron microscopy (SEM) and transmission electron microscopy (TEM), which revealed the uniform diameter of the sample (300–500 nm). In addition, it can be clearly seen that there are many pores connected to the internal space which enhance the electronic conductivity and shorten the ion transport channel. Owing to this unique structure, it shows excellent rate performance at various current densities. CF-Si/SiO_x-700 delivered a reversible capacity of 600 mA h g^{-1} and a capacity retention rate of 99% after 400 cycles, which represents its outstanding structural stability. In a similar manner, Zeng *et al.*[51] conducted a study where they utilized an Al/Si alloy as the raw material and employed selective etching with HCl to produce Al-doped porous Si/SiO_x composites (Fig. 3a). Multiple experiments were conducted at different HCl concentrations and durations to achieve the desired results. From SEM images, it can be seen that a uniform three-dimensional porous structure is formed, which can enhance the electronic and ionic conductivity (Fig. 3b). As the etching depth increased, there was a reduction in Si^{4+} and the outer layer acted as a protective barrier, thereby improving the cycling stability. The presence of residual Al plays a crucial role in enhancing the conductivity and preserving the porous structure. Furthermore, during the initial charge/discharge, the SiO_x outer layer undergoes various side reactions, leading to a significant decrease in the resistance of the battery system during subsequent cycles (Fig. 3c). In addition, the composite material exhibits a promising specific capacity of 2914 mA h g^{-1} at 0.1 A g^{-1} (Fig. 3d). Raza *et al.*[52] obtained porous $SiO_x/Mg_2SiO_4/SiO_x$ composites through high-temperature reduction of SiO by Mg. The introduction of silicate into this multilayer structure significantly improves the electrochemical reversibility and almost completely suppresses the volume change of SiO_x during electrochemical reaction. The porous structure of the composite not only ensures enough electrolyte and electron transport pathways, but also enriches the active sites on the surface.

Hollow SiO_x particles can fundamentally solve the intrinsic volume effect of SiO_x. Sufficient internal reserved space has been proved to be very effective in mitigating the dramatic volume change during delithiation.[53] Zhou *et al.*[54] judiciously used dialdehyde molecules, triaminopropyltriethoxysilane (APTES) and terephthalaldehyde (TA), as the precursor of carbon and Si, and synthesized polymer hollow spheres (PHSs) in one step through aldehyde amine condensation reaction (SiO_x/C HS-TA). Furthermore, the PHSs were obtained by using a crosslinking agent, and the size, morphology and carbon content could be precisely tuned (Fig. 3e). In addition, organic carbon and organosilicon in PHSs generate a carbon matrix and a SiO_x unit after high-temperature pyrolysis, resulting in the formation of an inherent ultra-fine hollow architecture (Fig. 3f). This SiO_x/C composite can not only alleviate the stress of cycling, but also result in excellent electrochemical performance in terms of reversible capacity, rate performance and coulomb efficiency (Fig. 3g). Xu *et al.*[55] proposed an environmentally friendly, efficient and simple route for preparing hollow SiO_x composites encapsulated by carbon conductive networks. With polyacrylic acid (PAA) as the soft template, TEOS was hydrolysed and condensed to form a SiO_2 layer. When the PAA template was immersed in an aqueous solution, it dissolved to form hollow SiO_2 spheres. Then, SiO_2 particles were mixed with phenolic resin, and a layer of carbon shell was formed in the carbothermal reduction process, while SiO_2 was reduced to the SiO_x matrix. Li *et al.*[56] reported a composite of self-assembled, metal organic framework (MOF) template induced hollow SiO_x nanoparticles coated with N-doped graphene aerogels. This nanocomposite possesses a 3D porous

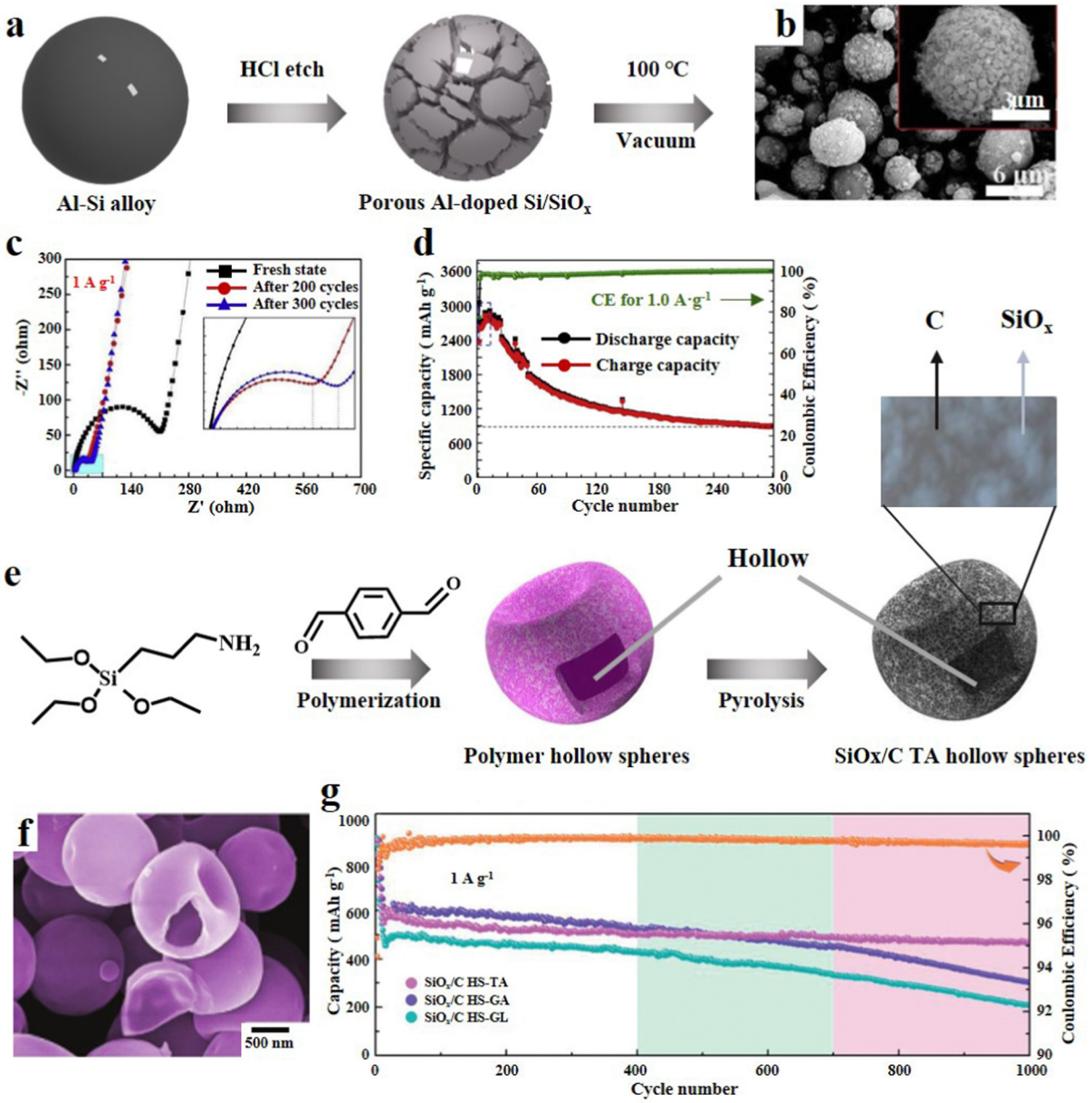

Fig. 3 (a) Schematic diagram of the synthesis of Al-doped porous Si/SiO_x, (b) SEM images, (c) EIS results and (d) cycling performance at 0.1 A g^{-1}.[51] Reproduced from ref. 51 with permission from Elsevier, Copyright 2020. (e) Schematic illustration of the synthetic procedure of SiO_x/C HS-TA, (f) SEM image and (g) long-term cycling performance at 1.0 A g^{-1}.[54] Reproduced from ref. 54 with permission from John Wiley and Sons, Copyright 2021.

structure with abundant pores and a high specific surface area, and exhibits rapid high Li^+ transport and electron transfer.

3.1.2. SiO_x nanowires. Devices based on SiO_x nanowires (SiO_x NWs) show further improvements in the 3D structure. In addition to the general advantage of resistance to strain, they also fundamentally improve the conductivity.[57,58] Furthermore, in general, a SiO_x NW device is directly connected to the current collector, thus reducing or even eliminating the need for an additional binder. SiO_x NW devices have a robust structure, which greatly inhibits the volume change during charging/discharging, which can reduce the decrease in capacity.[59] Li *et al.*[60] synthesized SiO_x NWs using a tie-assisted method. With low-cost mesoporous silica as the precursor, the loading of Fe^{3+} plays a crucial catalytic role within the pores. When subjected to ethylenediamine steam treatment, SiO_x NWs grow on the surface of SiO_x spheres along the direction of the lowest energy. Although the diameter and length of NWs increase during lithium insertion, this one-dimensional structure has strong structural integrity and remains intact without breaking into smaller particles throughout the cycling process. Additionally, the carbon coating can enhance the mechanical strain resistance and significantly improve the conductivity of the electrode. Kim *et al.*[61] reported a synthesis method in which polymethylsilane was thermally decomposed, resulting in the formation of SiO_x. This SiO_x material was then coated onto the surface of activated carbon nanotubes. The porous SiO_x layer

with a thickness of about 1 nm increased overall specific surface area of the material. The porosity can be modulated by adjusting the Si/C ratio and heat treatment conditions. The SiO_x nanotubes with a hollow structure have excellent rate properties due to the shortened Li^+ transport channel and reduced Li^+ transport length. The structure with a reserved inner void space can buffer the volume change of SiO_x during cycling. Wang *et al.*[62] synthesized a bamboo-like structured SiO_x/C composite by using polymer coating technology, which showed long cycle life and excellent structural integrity. Similarly, Liu *et al.*[63] prepared Si-void@SiO_x nanowires using a selective etching method combined with a thermal evaporation strategy. SiO_x after lithiation facilitated the formation of a stable SEI, and the void space allowed for extra expansion of Si. This special Si-void@SiO_x nanowire electrode exhibited outstanding lithium-storage performance, such as high reversible capacity and excellent cycling stability.

3.1.3. SiO_x nanofilms. SiO_x nanofilms typically exhibit a layered structure when used in conjunction with graphite and have found efficient utilization in LIBs. However, there are few research achievements on the SiO_x nanofilm anode material in LIBs, but it attracts more and more attention due to its small volume change during cycling.[64] The layered structure provides a transmission channel for Li^+ and greatly improves the performance. Moreover, the three-dimensional layered structure can significantly increase its stress-buffering capability. Takezawa *et al.*[65] synthesized a SiO_x film on roughened Cu through reactive evaporation. This SiO_x film shows excellent structural stability, as evidenced by the absence of significant particle pulverization during cycling. Despite the excellent performance of SiO_x nanofilms, the preparation process is still considered relatively immature and requires further exploration and refinement.

3.2. Oxygen content of SiO_x

Compared with Si based anodes, SiO_x based anodes have more stable cycle performance, which can be attributed to the addition of oxygen element, and the oxygen content has a critical influence on the performance of the anode.[66,67] Having a deep understanding of the effect of the oxygen content in SiO_x is indeed crucial for advancing the application of SiO_x-based anode materials in LIBs. Yang *et al.*[68] studied scientifically the effect of oxygen content in SiO_x (0.8, 1 and 1.1) as the anode material on the electrochemical cycle of LIBs. Through XRD results, crystalline Si, amorphous SiO, and amorphous SiO_2 phases were found in SiO_x, and it was proved that they all participated in the energy storage reaction with Li^+. The increase in oxygen content in SiO_x will diminish the insertion of lithium-ions, thus reducing the specific capacity of the material. However, the sacrifice of specific capacity alleviates the volume expansion of the electrode, thus significantly improving the cycle stability. Moon *et al.*[69] have provided valuable insights into the influence of oxygen content on the electrochemical performance of SiO_x through extensive theoretical calculations. Employing density functional theory (DFT) calculations, the Li–Si–O ternary phase diagram is obtained, which has practical significance to understand the reaction products between SiO_x and lithium (Fig. 4a). The increase in oxygen content will significantly affect the conductivity. According to the energy band theory, the oxygen content is proportional to the band gap (Fig. 4b). After further mathematical analysis, they speculated that, with the increase of oxygen content, there will be a higher voltage platform, which is more favourable for Li embedding. The voltage values of Si and SiO_x were compared in the experiment, confirming the accuracy of the theoretical calculation. By employing similar mathematical approaches, it is conjectured that as the oxygen content decreases, the propensity for SiO_x to undergo elastic softening increases, potentially leading to material disintegration.

Recently, Cho *et al.*[70] reported the effect of oxygen content on the structural evolution of SiO_x during electrochemical cycling. Thin films (50 nm) with different oxidation degrees were prepared by magnetron sputtering, and the changes of the SiO_x surface were investigated. The flow rate of oxygen/argon entering the chamber determines the oxygen content in the chamber. Thus, SiO_x films with different oxygen contents can be obtained. The films were also analysed by electrochemical analysis and *in situ* X-ray photoelectron spectroscopy (XPS). As shown in Fig. 4c, different oxygen contents will cause a voltage shift of peak 3, which is due to the oxygen related reaction inside the battery and is irreversible in the first few cycles (Fig. 4c). Peak 3 can be stable over about 30 cycles. However, with the increase of oxygen content, a higher voltage appears at peak 3. It is speculated that this is due to the inertness of Si–O, and the Si–Si after lithiation can be recycled reversibly, which increases the conductivity and capacity. When the SiO_x film is assembled into a half cell for testing, it can be clearly observed that, with the increase of oxygen content, the capacity retention rate increases, but the reversible capacity decreases as expected (Fig. 4d). Moreover, through the electrochemical impedance test of $SiO_{0.3}$, SiO and SiO_2, it is shown that the total resistance is significant, increasing with the increase of oxygen content, which is consistent with the analysis of the energy band theory. This is also due to the inherent insulation of the Si–O bond, and the difficulty of Si–O bond breaking hinders the diffusion of Li^+. Moreover, it can be seen from the EIS images that the overall resistance tends to decrease from the 25th cycle, which is a result of the activation of electrode materials. Similarly, the design of this nano-scale thin film makes it possible to observe the macroscopic changes of the electrode surface more clearly. By comparing the electrode materials with different oxygen contents after cycling, it can be seen that the high oxygen content makes the electrode material more difficult to crack. These advantages of high oxygen content can be attributed to the formation of a stable SEI, which has a certain buffering effect on the change of electrode volume.

Ge *et al.*[71] obtained SiO_x/C with different oxygen contents through a simple and scalable process. SiO_2 microspheres were prepared by hydrolysis and condensation of TEOS. Using hexadecyltrimethylammonium bromide (CTAB) as the template, porous SiO_2 was obtained after the soft template was

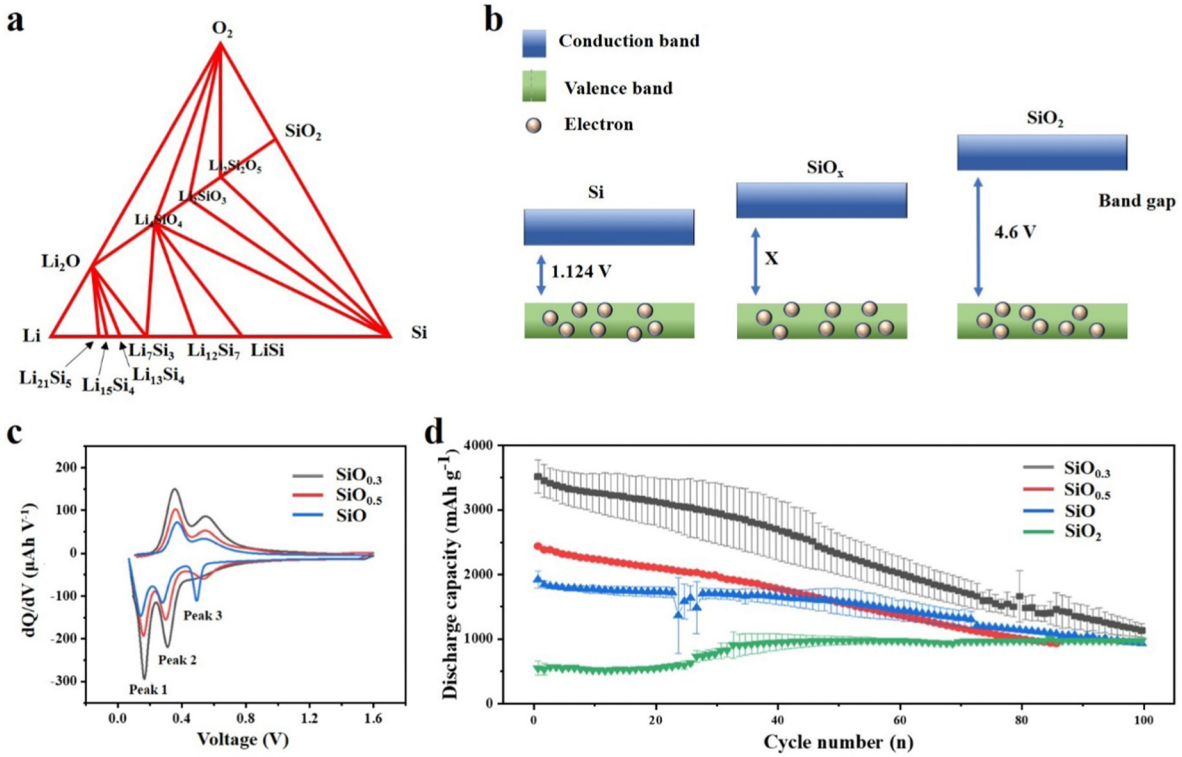

Fig. 4 (a) Ternary phase diagram of Si, O, and Li using density functional theory calculations.[69] Reproduced from ref. 69 with permission from John Wiley and Sons, Copyright 2020. (b) Band gap of Si, SiO_x and SiO_2. (c) dQ/dV curves of the 10th cycle data for three SiO_x films and (d) discharge capacity *vs.* cycle number of various SiO_x thin film electrodes over 100 cycles.[70] Reproduced from ref. 70 with permission from American Chemical Society, Copyright 2022.

removed by annealing in air. Subsequently, SiO_2 and Mg were mixed at different mass ratios and reacted at high temperature. HCl solution was used to remove the template MgO. Finally, SiO_x/C with different oxygen contents were obtained by polymerization of formaldehyde and resorcinol on the surface of SiO_x followed by carbonization. An appropriate amount of Mg can achieve good electrochemical performance. After 300 cycles, the best SiO_x/C composite possessed a capacity of 1010.4 mA h g^{-1} at 1 A g^{-1}. Cao *et al.*[47] reported a simple and cheap synthesis route to obtain SiO_x. Controlling the exposure time of Si powder to air during the milling process enables the manipulation of the oxygen content in SiO_x. Fan *et al.*[72] studied the diffusion and distribution of oxygen in SiO_x during heat treatment. After heat treatment of commercial SiO_x particles, it is found that oxygen will diffuse to the particle surface. During the process, an amorphous oxygen-rich layer forms around the SiO_x, while a crystalline Si core gradually develops within it. It is worth noting that the diffusion of oxygen in SiO_x can also be influenced by temperature. At higher temperatures, the diffusion of oxygen is enhanced, which can result in a more complete outward shift of oxygen from the SiO_x material. This means that the oxygen content of SiO_x can be adjusted by controlling the temperature during synthesis or processing. Furthermore, with higher temperature treatment, a larger pore structure will be formed after HF etching. Different etching times can also generate SiO_x particles with various pore sizes. This report serves as a theoretical foundation for the research and development of porous SiO_x materials.

4. Structural design of SiO_x/C composites

SiO_x has a high specific capacity, but its severe volume expansion and poor conductivity limit its further development and also lead to unrestricted growth of the SEI and electrode material pulverization (Fig. 5a).[73] The exceptional physical properties of carbon materials can be effectively combined with SiO_x to mitigate its volume expansion and enhance electrical conductivity. Moreover, the experimental results show that the combination of SiO_x and carbon materials is one of the most effective ways to improve the cycle performance of SiO_x.[74] The most widely adopted method for compounding SiO_x particles is by employing graphite as a coating material. Graphite has good ductility and thus it can be physically coated with a layer of carbon on the surface of Si particles.[75] It is very important to reasonably design the structure of the SiO_x/C composites because a small change in the 3D structure of the SiO_x/C composites will have a significant impact on the electrochemical performance.[76] The main structures are the core–shell structure, yolk–shell structure, and some other novel structures, such as the SiO_x embedded graphite layer structure,

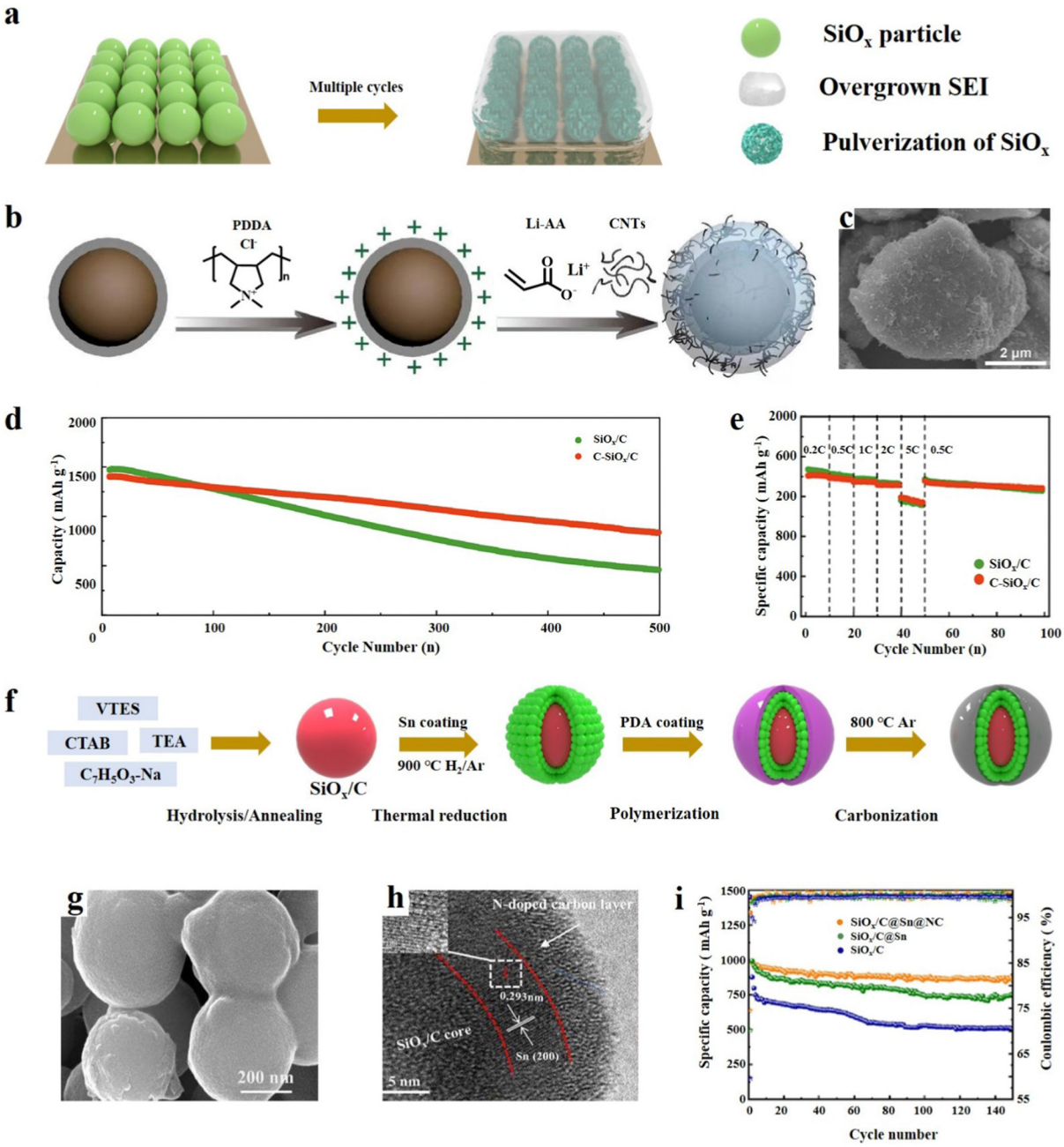

Fig. 5 (a) Schematic diagram of the failure mechanism of SiO_x based anode materials during cycling. (b) Schematic illustration of the preparation of C-SiO_x/C, (c) SEM image, and (d) cycling performance of Li‖SiO_x/C and (e) Li‖C-SiO_x/C at 0.2C for the first three cycles and at 0.5C for the subsequent cycles and rate capabilities.[15] Reproduced from ref. 15 with permission from Elsevier, Copyright 2020. (f) Schematic diagram of the preparative route for SiO_x/C@Sn@NC, (g, h) SEM and TEM images and (i) cycle performance at 0.2 A g^{-1}.[86] Reproduced from ref. 86 with permission from Elsevier, Copyright 2023.

nanotube structure, *etc.* The synthesis method and the characteristics of the structure–activity relationship are also described in the following.

4.1. Core–shell SiO_x/C

The SiO_x/C core–shell structure involves utilizing SiO_x as the core material and completely enveloping SiO_x with graphite. This approach enables the integration of the advantageous properties of both SiO_x and graphite, offering a synergistic strategy.[77] The carbon layer can not only efficiently buffer the volume change during cycling, but also significantly increase the electrical conductivity. Overgrowth and suppressed cracking of the SEI layer are considered crucial factors that significantly impact performance, and the tight coating of SiO_x with the carbon layer avoids contact between SiO_x and the electrolyte, thus forming a stable SEI film to enhance the cycle performance.

Gu *et al.*[78] demonstrated a simple way to coat SiO_x with polydopamine (PDA) with rich hydroxyl groups; PDA is able to form a stable carbon layer on the surface of SiO_x (SiO_x@PDA@GNH). The functional groups on dopamine can bond with the graphene nanotube hybrid (GNH) to form a hybrid layer, and the coating layer is evenly distributed and has good electrolyte wetting properties. Compared with SiO_x and SiO_x@PDA, the lithiation/delithiation voltage of SiO_x@PDA@GNH is obviously higher, resulting in a higher discharge power. It was found that SiO_x@PDA@GNH shows a significantly better cycling performance and has a capacity of 1269 mA h g^{-1} at 0.05C. After subjecting the SiO_x and SiO_x@PDA@GNH electrodes to 50 cycles of testing in half cells, significant differences were observed in their electrode structures as revealed by SEM analysis. The SiO_x@PDA@GNH electrode exhibited no noticeable signs of peel off or cracks, indicating its enhanced stability and structural integrity. Transition growth of the SEI and particle pulverization can lead to decreased coulombic efficiency (ICE), and storage performance may continue to degrade during repeated Li uptake/release cycles.[79] Li *et al.*[15] dispersed SiO_x/C and polydimethylammonium chloride (PDDA) in distilled water to coat SiO_x/C. Lithium polyacrylate (Li-PAA) was then formed on the surface under the initiation of ammonium persulfate, while simultaneously embedding MWCNTs to obtain C-SiO_x/C particles (Fig. 5b). Electron microscopy characterization revealed that the surface of the material particles is rough and porous, which may be a result of the embedding of polypropylene lithium and carbon nanotubes (Fig. 5c). The rate performance test showed that C-SiO_x/C has better electrochemical reversibility (Fig. 5d). Owing to the flexible Li–PAA interface, the material can maintain structural integrity during long cycling and continuously deliver high reversible capacity (Fig. 5e). Zhang *et al.*[80] developed an efficient and mild method to synthesise a core–shell SiO_x/C composite for LIBs. They mixed citric acid with SiO_x through ball milling and obtained a uniform core–shell structure material after carbonization. The SiO_x/C shows superb electrochemical performance with a high specific capacity of 1296.3 mA h g^{-1} and has a capacity retention of 65.1% after 200 cycles. The mild approach and excellent properties of SiO_x/C make its commercial large-scale production possible. Recently, Lee *et al.*[81] reported a method of physically combining SiO_x with graphene to form a durable and high-energy hybrid anode. Graphene shows strong ductility and good adhesion on the SiO_x surface, which can greatly reduce the volume expansion during multiple cycles. Thus, this synthesis method provides an efficient and simple method for the production of high-performance SiO_x anode materials. Although physical strategies for synthesizing SiO_x are simple and easy to operate, they can also result in the formation of many large defects on the surface of SiO_x. These defects can lead to direct contact between the SiO_x material and the electrolyte, which can cause the electrolyte to be consumed and result in the overgrowth of the SEI.[74] SiO_x can generate a uniform and dense coating on the surface by electrostatic interaction or chemical binding. Zhang *et al.*[82] designed a sol–gel method to synthesize SiO_x/C core–shell structure anode materials. They employed a wet-milling method to reduce the particle size of SiO_x, which can help to mitigate the volume expansion of the electrode material during the charge and discharge cycles. After 170 cycles, it still had 97.3% capacity retention. SiO_x particles were synthesized by Shi *et al.*[83] with equimolar amounts of Si and SiO_x by thermal evaporation. SiO_x was mixed with dopamine solution to obtain a SiO_x precursor coated with polydopamine. The polydopamine coating served as a carbon source during subsequent high-temperature carbonization, resulting in the formation of a SiO_x@C composite material. The carbon coating stabilized the structure of the material and contributed to the formation of a stable SEI, and the rate performance was significantly improved. At a current density of 0.1 A g^{-1}, the core–shell structure material exhibited a reversible capacity of 1514 mA h g^{-1}. Similarly, Lv *et al.*[84] reported a method to synthesize core–shell SiO_x/C nanostructured materials through sol–gel synthesis, which can achieve high yield and provide experimental guidance for industrial production. This SiO_x/C carbon layer was relatively thin and evenly distributed, and a specific capacity of 820 mA h g^{-1} could still be delivered after 100 cycles.

It is indeed worth noting that the research achievements primarily focused on single-layer carbon coatings. However, it has been observed that multi-layer coatings are more effective in mitigating the volume change of SiO_x, leading to improved cycle performance.[85] Li *et al.*[86] have developed a highly efficient anode material, SiO_x/C@Sn@NC, with a double-layer coating structure. This material exhibits outstanding electrochemical performance, and its preparation involves the hydrolysis of vinyltriethoxysilane (VTES) using the TEA ($C_6H_{15}N$) catalyst in a solution of sodium salicylate and CTAB to obtain a precursor. The precursor is then carbonized at high temperature, yielding SiO_x/C nanoparticles which are then coated with Sn and N-doped carbon (Fig. 5f). The SEM analysis confirms that the material is uniformly layered and coated, while TEM shows clear lattice stripes of Sn and amorphous N-doped carbon on the outermost layer (Fig. 5g and h). The combination of multiple active components and the double-layer coating structure significantly enhances ion diffusion and charge transfer, and promotes the formation of a stable SEI capable of absorbing stress during electrode cycling. Comparison studies reveal that both Sn and N-doped carbon can improve the specific capacity and cycling performance of the material (Fig. 5i). Wang *et al.*[87] designed a method to synthesize SiO_x/C@C through solvent-free ball milling and the sol–gel method. The whole synthesis process has no solvent participation, which reduces the risk of waste and potential pollution. Carbon encapsulation and doping jointly improve the electrochemical performance of SiO_x, showing a reversible capacity of 546 mA h g^{-1} after 1000 cycles at 1 A g^{-1}. Similarly, Guo *et al.*[88] designed a bilayer structure in which the Si–SiO_x particles were coated with carbon and a polymer. Each layer of coating has a specific role, and the main effect of the inner layer of carbon coating is to improve the conductivity. The outer layer of the composite material can take advantage of the elasticity of the polymer, can well limit the

volume expansion of Si–SiO_x and enhance structural integrity during cycling. In the half cell test, the materials exhibited a stable capacity of 794 mA h g^{-1} at 2C after 900 cycles and a capacity retention of 83%. Moreover, in the full battery test, the capacity loss was only 20% after 1100 cycles. In addition to bilayers of carbon, SiO_x itself can also be used as a shell. Zhou *et al.*[89] designed a double-layer structure with an inner layer of SiO_x and an outer layer of diatomic co-doped carbon layer. The inner layer SiO_x here also acts as a buffer layer to control the volume change of the Si core, and the outer carbon layer rich in defects acts as a conductive layer. Together, the two layers can significantly improve the electrochemical performance of the material. Zhu *et al.*[90] reported a homogeneous multilayer core–shell structure Si@SiO_x@C material, in which Si was coated with SiO_x and soft carbon. The thickness of SiO_x can be adjusted to 2–15 nm through adjusting the calcination temperature. The multilayer structure protects the Si particles during cycling, thus enhancing the structural integrity, and significantly improves the conductivity.

As a novel and efficient SiO_x/C composite structure, the porous carbon layer coating structure has attracted extensive attention. The porous carbon layer acts as a conductive matrix and can be used as a buffer layer to reduce the volume expansion of SiO_x to enhance the cycle stability. The structure can reduce the length of the diffusion path of Li-ions and enhance the conductivity between electrolyte and electrode materials. Zhang *et al.*[91] reported a porous P@C/SiO_x core–shell structure material; the activated material showed a reversible specific capacity of 1151.8 mA g^{-1} at a current density of 0.1 A g^{-1} and an excellent ICE of 79.2%. However, the coulomb efficiency of carbon coated rice husk without treatment was only 45.7%. Similarly, Cui *et al.*[92] also used rice husk as both Si and carbon sources to obtain mesoporous SiO_x/C core–shell composites by carbothermic reduction of precursors. In the half battery test, the capacity attenuation of the material was less than 0.5% after 200 cycles, making it a good substitute for the graphite material. Despite the notable enhancement in electrochemical performance achieved with the use of porous coatings, the design of the coating structure for a porous carbon layer remains a challenging task. Currently, there is no well-established method for creating the desired porous structure and regulating the pore size, necessitating further experimental investigations by researchers.[93]

4.2. Yolk@shell SiO_x/C

The yolk–shell structure is a distinctive structure based on the core–shell structure and leaves a certain space between the carbon layer and the SiO_x core.[94] The conventional tightly wrapped structure is limited in its ability to fully control the expansion of SiO_x, which can potentially result in the cracking of the carbon layer and even structural collapse.[95] The design of reserved buffer space can allow the SiO_x core to shrink more freely, and the SEI film and even the entire electrode structure can maintain good integrity, thus enhancing the cycle stability (Fig. 6a).[96] The yolk–shell structure is usually synthesized by the sacrificial template method. Cui *et al.*[97] first reported the Si anode material with yolk shell structure. They synthesized a kind of amorphous carbon as the shell, which was coated on the Si nanoparticles by the sol–gel method. This yolk–shell structure benefits from this layer of SiO_2 as a sacrificial layer. This layer of SiO_2 is finally etched with HF to form the gap, so the thickness of SiO_2 can determine the size of the final void space. Tactfully, it can be adjusted through experimental methods to achieve controllable SiO_2 thickness. It was found that the sacrificial coating thickness should be larger than 30 nm to reserve enough space, so that the outer carbon shell will not be damaged when Si expands. However, this layer of void space cannot be too large, which will reduce the bulk density. The material exhibits a specific capacity of 2800 mA h g^{-1} at a C/10 current density.[97]

Liu *et al.*[98] synthesized SiO_x/C composites with a yolk@shell structure through the sol–gel process and selective etching. Three kinds of SiO_2 with different functional groups (–SCN, $–CHCH_2$ and –SC) were formed by hydrolysis and condensation of different silanes and coated layer by layer. First, cyano containing silane was hydrolysed to synthesize SCN-SiO_2 microspheres, which were then coated. The middle layer is CH_2CH–SiO_2 and the outer layer is SC-SiO_2. The ingenious thing is that the $–CHCH_2$ of the intermediate layer shows weak alkalinity, which can be removed by the selective reaction of hot sodium hydroxide, thus forming a precursor with a yolk@shell structure (SiO_2@void@SH-SiO_2). After high temperature annealing in an Ar atmosphere, the organic phase converted into amorphous carbon, and finally SiO_x@void@C was obtained. The chemical vapor deposition (CVD) technology is used for annealing in flowing acetylene and argon to form a uniform semi-graphitized carbon layer in the outer layer of SiO_x (Fig. 6b). The void space can be clearly seen from the TEM images (Fig. 6c). The incorporation of a semi-graphitized carbon layer serves a dual purpose: it enhances the electron diffusion rate and addresses the issue of traditional carbon layers being prone to cracking. This unique yolk@shell structure contributes to the exceptional electrochemical performance of the material, particularly its impressive rate performance. In the first 150 cycles, the capacity attenuation is only 3%, and under a high current density of 1 A g^{-1} the discharge capacity is 725 mA h g^{-1} (Fig. 6d). Interestingly, the capacity increases after 200 cycles, which is mainly due to the reversible side reaction between the electrolyte and electrode materials. Moreover, NaOH solution is used to remove the silica layer, which is safer and more environmentally friendly than traditional HF etching.[99] In addition, the design of a semi-graphitized carbon coating can also provide some experimental reference for other anode materials with an obvious volume effect.[100]

The incorporation of a double-layer carbon shell remains an exceptionally efficient structural design concept within the yolk@shell structure.[101] Recently, Luo *et al.*[102] synthesized a new type of bilayer yolk@shell SiO_x@C@C anode material by a hydrothermal method. Firstly, Si nanospheres were obtained by hydrolysis and condensation of vinyl triethoxysilane, which were then annealed in an argon atmosphere to form SiO_x/C composites. A surface modifier (PDDA) was used to treat the

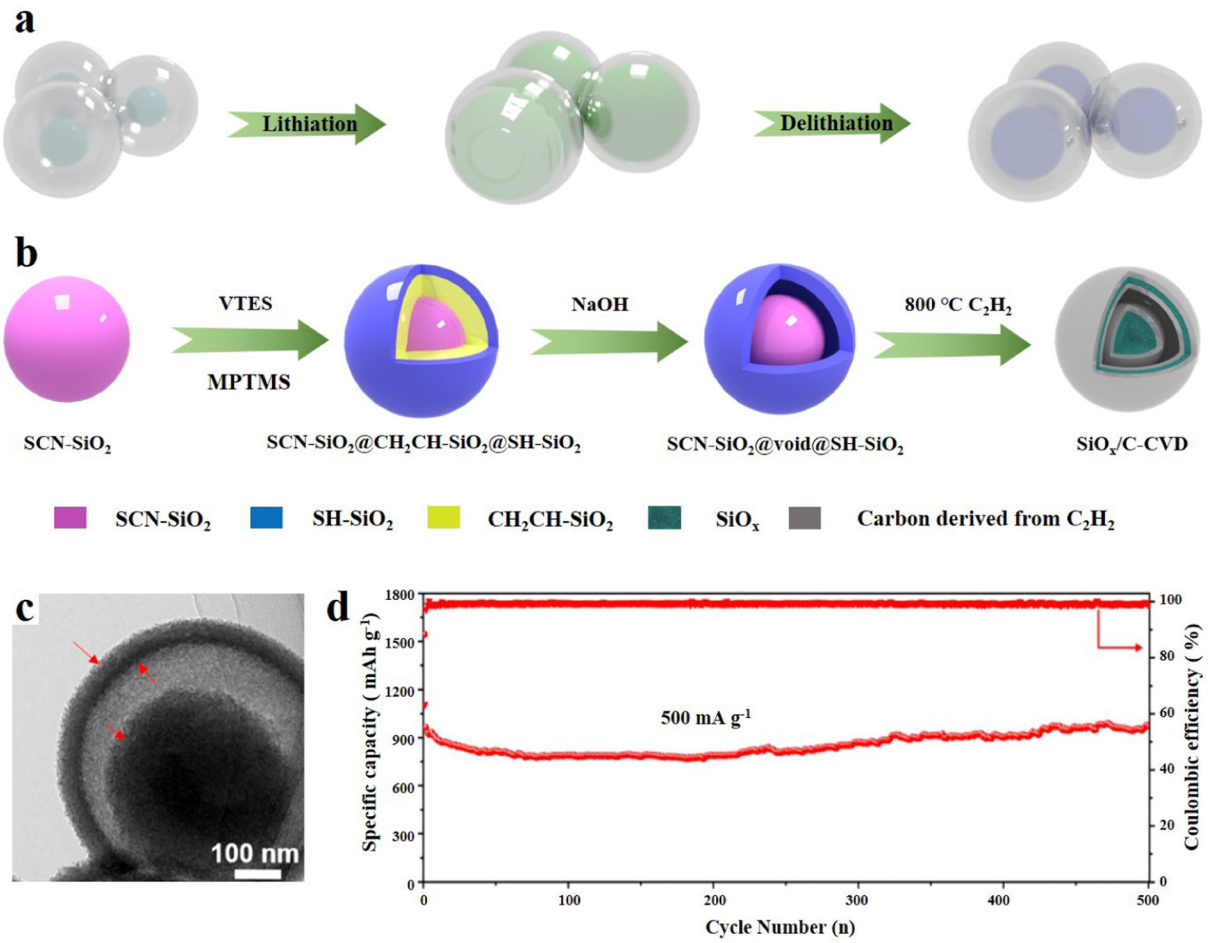

Fig. 6 (a) The evolution of the yolk@shell structure during lithiation/delithiation. (b) Schematic illustration of the preparation of SiO_x/C-CVD, (c) TEM image and (d) long-term cycling performance at 500 mA g^{-1}.[98] Reproduced from ref. 98 with permission from Elsevier, Copyright 2019.

surface of SiO_x balls, so that a layer of methyl methacrylate (PMMA) can be coated on their surface. The formation of the yolk@shell structure is because the PDDA in the middle layer will self-react and release gas during high temperature treatment, resulting in a cavity in the overall structure. The conductivity of SiO_x can be significantly enhanced by incorporating additional internal carbon shells in its structure. Moreover, the design of a double layer carbon shell aids in the formation of a more stable SEI film. The uniform coating of the inner carbon shell on the core effectively prevents undesired side reactions between the electrolyte and SiO_x, thereby minimizing electrolyte consumption. Based on the above findings, the yolk@shell structure shows superior capacity and cycle performance to the core–shell SiO_x/C@C structure. After 500 cycles at 0.5 A g^{-1}, the material exhibits a discharge capacity of 770 mA h g^{-1}, with an ICE of 99%. Wang *et al.*[103] synthesized yolk@shell N,S co-doped SiO_x/C@void@C by a one-step method. Co-doping based on the double-layer carbon shell further improves the overall conductivity, and the material still has 464 mA h g^{-1} energy density under a high current density of 5 A g^{-1}. The combination of a simple and efficient synthesis method and the demonstrated excellent electrochemical performance firmly establishes this material as a highly promising candidate for anode materials in LIBs.

Environmentally friendly synthesis routes hold greater practical value.[104] Zhang *et al.*[105] developed a HF-free method to synthesize a yolk@shell structure SiO_x/C@C composite. Two layers of the polymer shell are generated on the Si core, and the middle layer is polydopamine, which can be selectively etched by NaOH to form voids. The outer layer of polypyrrole can form a N-doped carbon shell after carbonization at high temperature, which greatly improves the conductivity. This composite can still provide 804 mA h g^{-1} capacity at 0.1 A g^{-1} after 1000 cycles. Recently, Chen *et al.*[106] also designed a HF-free strategy to synthesize a new type of SiO_x/C@void@Si/C yolk@shell structure. SiO_2 containing vinyl is synthesized through a hydrothermal reaction, and upon vinyl carbonization, amorphous carbon is formed. This amorphous carbon can create a core–shell structure, with SiO_x embedded within it. Through the use of molten $AlCl_3$, metal Al is then able to reduce SiO_2 at low temperatures, resulting in the generation of Si. As Ostwald ripening occurs, the newly formed Si diffuses outward and merges, ultimately forming a perfectly spherical structure. With a sufficient reaction time, a void space is created between

layers, forming the yolk@shell structure. In addition, the gap size of the void space can be effectively adjusted by the time of aluminothermic reduction. The synergistic effect of the two layers of carbon not only enhances the conductivity, but also mitigates the effect of the volume change of SiO_x and Si in maintaining structural integrity. SiO_x/C@void@Si/C shows excellent cycle stability. After 550 cycles, there is an initial reversible specific capacity of 1093 mA h g^{-1} at 0.2 A g^{-1}. Similarly, Gong *et al.*[107] reported a unique SiO_x@TiO_2@C negative electrode material. Tetrabutyl titanate was hydrolysed to coat TiO_2 on the surface of SiO_x by the sol–gel method, and phenolic resin was formed on the surface of SiO_x by the reaction between resorcinol and formaldehyde, and a carbon shell was formed after calcination. TiO_2 is a typical amphoteric oxide that can be etched by NaOH to avoid the environmental harm caused by HF. Furthermore, the size of the void space can be adjusted by varying the etching time. By adapting well to the volume expansion of SiO_x, TiO_2 can effectively enhance the electrochemical performance. A specific capacity of 1290 mA h g^{-1} is delivered under a current density of 0.1 A g^{-1}.

4.3. Novel structures of SiO_x/C

The SiO_x/C composite exhibits a distinctive and adaptable structure–activity relationship.[50,108] The addition of carbon not only improves the conductivity of SiO_x, but also maintains the micro-integrity of the electrode material.[109] The continuous exploration of the SiO_x/C structure has led to the steady optimization of the physical and electrochemical properties of SiO_x based anode materials.[110] The core–shell structure and yolk@shell structure of SiO_x/C have been previously discussed, highlighting their structural characteristics and performance characteristics. Furthermore, SiO_x/C composites showcase a wide array of structures that go beyond the aforementioned types, and demonstrate exceptional performance.[111]

4.3.1. Pomegranate-like structured SiO_x/C. The pomegranate-like structured SiO_x/C composite is an advanced material that is based on the yolk@shell structure. Due to the relatively large hollow volume and specific surface area inherent in the yolk@shell structure, it is inevitable that the tap/packing density of the electrode will be reduced. The pomegranate-like agglomerated structure, characterized by interconnected single carbon shells, significantly enhances the conductivity of the materials. This interconnected network of carbon shells effectively increases conductivity while reducing the contact area between the electrolyte and SiO_x. In addition, agglomeration can enable the particles in the inner layer to be coated and protected by the outer layer, enhancing the cycle stability. Yu *et al.*[112] synthesized ultrafine SiO_2 particles by hydrolysis and condensation of tetrapropyl orthosilicate, and synthesized phenolic resin *in situ* by a one-pot method. Subsequently, the surface of SiO_2 was modified by CTAB, so that the surface of phenolic resin could be uniformly coated. The SiO_x/resin mixture was dispersed in deionized water and then agglomerated using the spray drying method. Subsequently, the resulting agglomerates were subjected to high-temperature carbonization, leading to the formation of pomegranate-like SiO_x/C particles. As-prepared SiO_x/C has a uniform diameter of approximately 40 nm, with multiple particles agglomerating into a uniform sphere. The amorphous carbon layer enhances the overall conductivity and endows the composite with excellent lithium storage properties, delivering 1024 mA h g^{-1} after 200 cycles at 0.5 A g^{-1}.

4.3.2. Layered structure SiO_x/C. Compared with the spherical structure, layered structure SiO_x/C has attracted extensive attention from academia due to its excellent transport performance of electrons and ions.[113] To synthesize a layered material with excellent performance, it is necessary to control the thickness, chemical composition and stacking order of the coating through an efficient chemical process.[114] The volume change of SiO_x has been reduced twice as much as that of Si, but the volume effect of 160% is still not ideal, which cannot meet the needs of industrial production. It is found that the layered structure can adapt to the volume change during cycling and buffer the internal stress by reducing the thickness of the film.[115] In recent years, the SiO_x/SiO_y layered structure materials reported by Zhang *et al.*[116] were superimposed by silica with different oxygen contents. By using a photoresist as the sacrificial layer, the Si particles and silica particles were respectively evaporated onto the sacrificial layer using an electron beam evaporator. The oxidation degree of Si could be controlled by controlling the partial pressure of oxygen, and the thickness of the coating could also be controlled. Finally, the photoresist was removed by etching with acetone. The greatest advantage of this approach is that the synthesis method is simple and the cost is low. This compact film design has higher loading density and area specific capacity compared to traditional layered electrode materials. In this work, the oxidation degree of silicon oxide is controlled by simple experimental means in order to control the performance of the materials. The outer layer of the double-layer structure is amorphous oxygen rich SiO_x ($x \sim 1.85$). The mechanical properties of SiO_x can be improved with the increase of the oxygen content, providing mechanical support and strain buffer function. However, the SiO_y in the inner layer has a low oxidation degree ($y \sim 0.5$) and realizes lithium storage with high capacity. The SiO_x/SiO_y electrode exhibited a high initial reversible capacity of 1474 mA h g^{-1} at 0.1 A g^{-1}. Furthermore, Xu *et al.*[117] developed a novel fabrication approach to synthesize graphite-like structure SiO_x/C composites. SiO_x particles were dispersed in the aqueous solution of graphene oxide (GO), and SiO_x/C was synthesized by the hydrogel method. Then, it was mixed with flake graphite (FG) and chitosan, and a suspension of SiO_x/GO/FG was formed under the electrostatic power effect. After centrifugation, the SiO_x/GO/FG composite can be separated (Fig. 7a). In this report, when the composite is immersed in emulsified asphalt, asphalt will be adsorbed on the composite. Finally, due to the shrinkage characteristic of asphalt at high temperature, the original structure of artificial graphite can be restored after high-temperature calcination. During the half cell test, SiO_x/C anodes exhibited excellent cycle and rate performance, with rate capabilities tested at various current densities, and the SiO_x/C anodes delivered a high capacity of

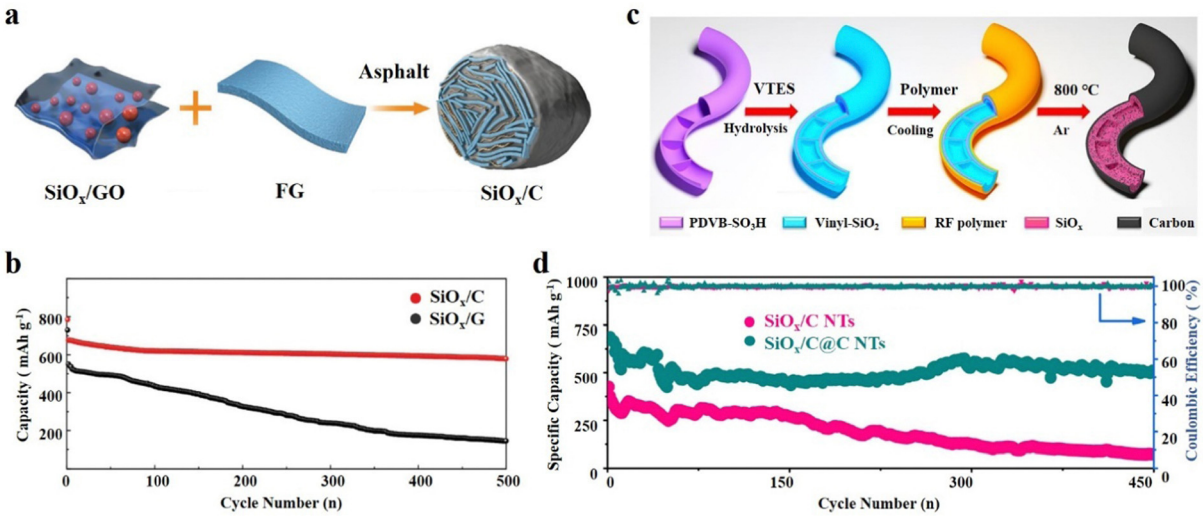

Fig. 7 (a) Schematic illustration of the synthetic process of the SiO_x/C hydrogel and (b) cycling performance.[117] Reproduced from ref. 117 with permission from John Wiley and Sons, Copyright 2017. (c) Schematic illustration of the preparation process of SiO_x/C@C NTs and (d) the long-term cycling performance at 500 mA g^{-1} of SiO_x/C@C NTs.[120] Reproduced from ref. 120 with permission from Elsevier, Copyright 2022.

580 mA h g^{-1} at 0.5C after 500 cycles (Fig. 7b). Moreover, the synergistic effect of multifarious carbon materials greatly improves the inherent defects of SiO_x based anodes, especially by forming a stable SEI and maintaining the integrity of electrode materials, and thus they can achieve good cycling performance under high current conditions.

4.3.3. Nanotube SiO_x/C. In addition to the above novel structures, the nanotube SiO_x/C anode material is also an efficient and potential structure. The nanotube structure is more suitable for electron transfer, and the hollow structure can also buffer the stress of SiO_x.[118] Recently, Wang *et al.*[62] reported a bamboo-like SiO_x/C nanotube composite. This hollow tubular SiO_x is a result of cationic polymerization, and the bamboo-like structure is realized by the free movement and periodic pause of the initiator in the polymerization process. The intermittent polymerization makes the nanotubes form uniform partitions, that is, a structure like bamboo knots. Bamboo knots playing a supporting role can serve a self-buffering function and improve the integrity of hollow structures. Then VTES was hydrolysed and condensed under the catalysis of the sulfonic group to form vinyl SiO_2 coated nanotubes. Finally, a layer of phenolic resin was coated on the nanotubes by a polymer coating process. After high-temperature calcination, vinyl-SiO_2 is converted into carbon and SiO_x, and the outer carbon shell is carbonized by phenolic resin (Fig. 7c). The nanotube has a high aspect ratio, and the Li^+ transmission length is greatly shortened. With the cooperation of the outer carbon layer, the electronic conductivity and ionic conductivity are improved at the same time. This bamboo-like architecture displayed a large reversible capacity of 511 mA h g^{-1} at 0.5 A g^{-1} after 450 cycles (Fig. 7d). In addition, in this hollow tubular structure, the stress can be released during cycling, and the structural integrity can be maintained well. Very recently, Xue *et al.*[119] fabricated a unique nanotube structure in which hollow carbon nanotubes were hybridized with ultra-fine SiO_x particles. Carbon nanotubes can not only provide electronic transmission, but also buffer the volume change of SiO_x. Benefiting from this structure, the material shows excellent electrochemical performance and delivers a specific capacity of 544 mA h g^{-1} after 500 cycles at 1 A g^{-1} current density.

5. Rational design strategy for SiO_x/C

5.1. Carbon types in SiO_x/C

During charging/discharging, volume expansion and contraction can lead to mechanical damage and a decrease in the electrochemical performance of the electrode material.[121,122] Carbon materials have good ductility and conductivity, and their composites with SiO_x effectively alleviate the inherent shortcomings of SiO_x, greatly promoting the development of SiO_x/C composite materials.[123] Due to the excellent performance of carbon materials and their abundant reserves on the Earth, researchers have developed various allotropes of carbon, such as graphene, carbon nanotubes, and fullerenes, by utilizing biomass, polymer carbonization, *etc.* (Fig. 8a and b). Different carbon types in SiO_x/C composites have unique physical and chemical properties, and there is desirable method to composite each carbon materials with SiO_x.[124] For example, graphene and carbon nanotubes are suitable for mechanical mixing and co-precipitation, while polymer carbonization is more suitable for the sol–gel method. The currently commercialized SiO_x/C material is a composite of SiO_x and carbon materials added to graphite or graphene through a specific process.[125] However, the amount of SiO_x added is still relatively low, resulting in a lower specific capacity of the composite material.[126,127]

5.1.1. Graphite. Graphite is a highly accessible and cost-effective form of carbon that finds widespread use in SiO_x/C

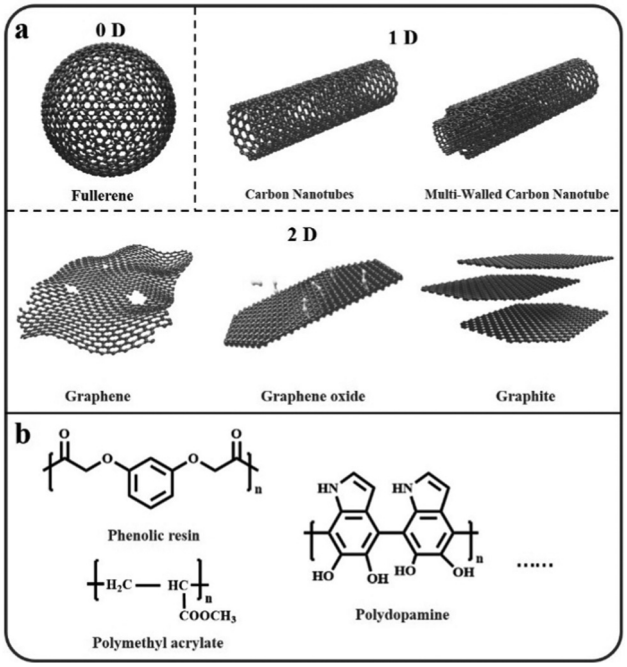

Fig. 8 (a) Commercial carbon materials for SiO_x/C composites. (b) Several carbon material precursors.

composites. It can be sourced from natural or artificial sources, with the former being a mineral that typically forms within rocks, while the latter is usually produced through high-temperature synthesis or chemical vapor deposition.[128] In industrial settings, graphite and SiO_x are typically blended and bound together using binders through mechanical means. The hybridization of amorphous carbon and SiO_x can be achieved through the carbonization of various polymers. Among these methods, *in situ* synthesis of phenolic resin is commonly employed. This approach allows for the simultaneous formation of amorphous carbon and SiO_x within the composite material.[129] It is possible to uniformly coat the surface of SiO_x with phenolic resin, resulting in a dense conductive structure after carbonization. Ouyang *et al.*[130] have developed a sequential coating approach to construct a hollow SiO_x anode material with a sandwich structure. They synthesized ZIF-8 with a nanotube structure by adding 2-methylimidazole and CTAB to a zinc ion-containing aqueous solution. A layer of SiO_x was formed by hydrolysing a Si source on the outer layer, creating ZIF-8@SiO_x. Subsequently, resorcinol and formaldehyde were added to form a phenolic resin on the surface of the material through a polymerization reaction. The sacrificial template ZIF-8 of the inner layer was calcined to form a porous N-doped carbon network, which both formed a hollow structure to buffer volume changes and significantly improved conductivity. The outer RF was thermally decomposed into amorphous carbon, which synergistically improved the electrochemical performance of the material with the inner carbon. This material could deliver a capacity of 583 mA h g^{-1} at a high current density of 1 A g^{-1}. Hu and colleagues polymerized 3-aminophenol and hexamethylenetetramine under heating conditions, coated the resulting product with SiO_x, and obtained a uniform carbon shell after annealing in an argon gas atmosphere.[131] Similarly, Zhou and colleagues polymerized and carbonized boric acid and aniline, leading to the generation of N-doped carbon on the surface of the material. In addition to *in situ* synthesis of polymers, incorporating organic carbon sources and subsequently carbonizing them to form a conductive shell is a concise and practical method.[84] Chang's team developed an $SCCO_2$-assisted coating method to achieve the composite of SiO_x with different organic substances. They compared the electrochemical performance by using glucose, sucrose, and citric acid as precursors and found that carbon deposited by $SCCO_2$ had fewer oxygen functional groups, making the material more conductive. When using glucose as a precursor, it showed the lowest resistance and the highest tap density.[132] Sun *et al.*[133] used pitch-derived carbon to synthesize carbon materials with different crystal structures and explored the influence of the microstructure of carbon on the lithium storage behaviour of SiO_x/C anodes. The higher the disorder degree of the microstructure of carbon, the greater the capacitance contribution of the electrode, thus exhibiting better electrochemical performance. However, a higher disorder degree will lead to increased specific surface area and defects in the full battery, which will consume more lithium and irreversibly affect the electrochemical performance of the full battery. The increase in the disorder degree of carbon will also lead to a decrease in the output voltage. This achievement provides a reference for developing high-performance SiO_x/C lithium-ion battery negative electrode materials using low-cost biomass due to the renewable nature of carbon as a natural resource.

The development of high value SiO_x/C composites using inexpensive biomass has gained attention due to renewable and rich reserves of carbon in nature. Biomass is often used as both a Si source and a carbon source, and biomass can be easily carbonized at high temperatures to obtain graphite like materials.[134] Yu's team utilized sugarcane leaves as raw materials and employed a molten salt-assisted low-temperature aluminothermic reaction to prepare a porous Si–SiO_x@Cu composite material.[135] They mixed sugarcane leaf powder with $CuCl_2$ and $ZnCl_2$ and calcined the mixture under an argon atmosphere. After thoroughly washing away the chloride salt with HCl and drying, they obtained a porous SiO_x/C precursor. The precursor was reacted with the mixture of $AlCl_3$ and Al powder in an argon atmosphere, and Al and Al-containing composites were washed away to obtain Si–SiO_x@C. The oxygen content of Si can be adjusted by varying the amount of aluminium powder added. After 400 cycles, a reversible capacity of 1562.8 mA h g^{-1} was observed at 0.2 A g^{-1}. Similarly, Chen and colleagues prepared layered porous carbon-coated SiO_x/C composites using bamboo shoot shells as raw materials.[136] Guo *et al.*[137] employed dried bamboo leaves to directly calcine and generate the SiO_x/NC precursor which was then calcined to produce N-doped carbon. The precursor was then subjected to a hydrothermal reaction with $Ni(OAc)_2{\cdot}4H_2O$ to obtain $Ni_3Si_2O_5(OH)_4$/NC, which was further used to prepare a series

of Ni/SiO_x/NC composite anodes by calcination at varying temperatures. It is worth noting that animal protein can also produce doped carbon during the calcination process, which significantly enhances the overall conductivity of the material. On the other hand, Meng and team surface-treated commercial Si powder to obtain Si@SiO_x, which was mixed with egg white and transferred to polytetrafluoroethylene hydrothermal kettle for molecular cooking. Finally, the product Si@SiO_x@C was obtained by calcination in a tube furnace. The outer layer of N-doped carbon not only enhances the conductivity but also maintains the interface stability of the electrode material. This double-layer structure effectively acts as a buffer, alleviating the internal strain experienced by the Si core during cycling.[138]

5.1.2. Graphene. Graphene is a single-layer mesh structure material composed of carbon atoms, which has strong mechanical strength, chemical stability, and high electrical conductivity.[139] Currently, construction of SiO_x/graphene composites is one of the most common and efficient strategies. However, building SiO_x/graphene composite materials through mild methods is still a challenge because the integrity of the graphene conductive network is crucial in mild synthesis environments.[140] Xue *et al.*[141] found that adding TiO_2 during the ball milling of graphite can produce multi-layer graphene (MLG). This mild method can effectively modify SiO_x and obtain SiO_x/TiO_2@MLG anode materials. SiO_x/TiO_2@MLG shows high lithium storage performance and cycling stability with a capacity of 1484 mA h g^{-1} and up to 1200 cycles at a current density of 2 A g^{-1}. The inclusion of TiO_2 in SiO_x can effectively mitigate the volume expansion effect and electrolyte decomposition during charge and discharge cycles. This unique capability is challenging to achieve with other metal oxides. Lee *et al.*[142] utilized commercial graphite foils to prepare graphene nanosheets *via* electrochemical exfoliation, which were then dispersed in *N*,*N*-dimethylformamide. By adding surface-treated SiO_x particles and co-sonicating with graphene, they obtained a SiO_x@Gr composite material with a graphene content of only 3 wt%, significantly increasing the 'specific capacity of the electrode material. The exceptional physical properties of graphene play a crucial role in mitigating the volume expansion of SiO_x during cycling. This effect leads to a significant improvement in the initial coulombic efficiency. Lee and colleagues investigated the electrochemical performance of SiO_x@Gr/AG as an anode material in lithium-ion batteries and achieved promising results. This improvement can be attributed to the adaptive behaviour of graphene, which reduces damage to AG during cycling and maintains good electron transfer pathways. Although graphene can significantly enhance the electrochemical performance of SiO_x, achieving a tight bond between the two materials through mild methods is challenging because the simple van der Waals force is the only interaction between them, and the structure of graphene is difficult to maintain. However, graphene can react with strong oxidants such as HNO_3 and H_2O_2 to oxidize some carbon atoms into functional groups such as carboxyl or hydroxyl, which can form chemical bonds with SiO_x, enhance mechanical performance and chemical stability, and maintain excellent structural integrity during charge and discharge processes. Xu *et al.*[94] also reported a new method to embed SiO_x particles into multi-layered reduced graphene oxide through self-assembly. The combination of SiO_x and traditional carbon materials will make the material connection unstable and loose, reducing the compaction density. Moreover, disproportionation reaction is easy to be caused during high temperature annealing, which reduces the specific capacity of materials. The combination of SiO_x with reduced graphene oxide (rGO) through the electrostatic effect, SiO_x particles are uniformly dispersed among the layers of rGO. When chitosan and graphene undergo a reaction at high temperatures, it enables the N doping of graphene. This process introduces N atoms into the graphene lattice, which increases the density of defects in the material. The incorporation of defects in graphene can optimize its electronic conductivity. Through physical property characterization, it can be found that the agglomeration of SiO_x particles is reduced, and they show good mechanical properties. The SiO_x particles embedded in graphene can greatly decrease the exposure sites, reduce the contact area between the electrolyte and SiO_x, and form a more stable SEI. SiO_x@C can maintain 80% of the initial capacity of 780 mA h g^{-1} after 1000 cycles at 1 A g^{-1}.

5.1.3. Carbon nanotubes. Carbon nanotubes (CNTs) are nanoscale materials that consist of carbon atoms arranged in a tubular structure, resembling rolled-up graphene sheets.[143] They can be classified into two types: single-walled carbon nanotubes and MWCNTs. With diameters in the nanometer range and lengths up to several micrometers or longer, carbon nanotubes possess excellent electrochemical properties and mechanical strength.[144] These unique characteristics make them highly desirable for various applications requiring high-performance materials. When CNTs are combined with SiO_x, they can effectively enhance the conductivity and mitigate volume effects in composite materials. Various methods are available for the preparation of SiO_x/CNT composites, including chemical vapor deposition (CVD), chemical *in situ* growth, and mechanical mixing. Tian *et al.*[18] used CVD to generate carbon nanotubes on particle surfaces, leading to improved reversible capacity. By reacting TEOS, $(Co(CH_3COO)_2{\cdot}4H_2O)$ and 2-methylimidazole to form uniform fumed SiO_2 and then hydrolysing TEOS to coat an outer layer of SiO_2, SiO_x@CNT/C was obtained through *in situ* growth of carbon nanotubes from C_2H_2/Ar under a H_2 atmosphere after SiO_2 reduction. Co particles wrapped in carbon layers were found at the tips of carbon nanotubes, and the authors suggested that Co particles catalysed the generation of CNTs. The SiO_x@CNT/C particle size and carbon nanotube length varied significantly at different CVD temperatures, and 550 °C was found to be the most appropriate. The hollow structure can mitigate volume expansion during the cycling process and enhance the cycling performance. *In situ* grown carbon nanotubes further enhance the mechanical strength and conductivity. Additionally, Co can inhibit the growth of the LiF-rich SEI and improve the initial coulombic efficiency. Similarly, Xue *et al.*[119] used self-catalysis to grow carbon nanotubes on SiO surfaces in an C_2H_2/Ar

atmosphere, partially reduced SiO with H_2, and achieved a tight connection between SiO_x and CNTs, which was a cost-effective approach compared to simple mechanical mixing methods. MWCNTs consist of multiple carbon nanotube cylinders, with a certain distance between layers, providing higher mechanical strength and stability than single-walled carbon nanotubes. Ren *et al.*[145] designed a process route to improve the electrochemical performance of SiO_x with N-doped carbon and MWCNTs. By dispersing a certain amount of MWCNTs in CTAB solution, adding ethyl silicate, collecting the precipitate, and then adding PAN and *N*-methylpyrrolidone (NMP) to encapsulate the material with a polymer, followed by high-temperature carbonization, the outer layer polymer was transformed into N-doped carbon, and SiO_x/MWCNTs/N-doped C was obtained. The material has a porous scaffold-like structure, greatly improving the conductivity. N-doped carbon also improves the electrical contact between particles, reducing material adhesion and agglomeration. Furthermore, electrochemical testing has demonstrated a significant improvement in the cycling stability and rate performance of SiO_x/CNT composites. At a current density of 0.1 A g^{-1}, the composites can deliver a stable capacity of 620 mA h g^{-1}. However, due to the complexity of the composite process between SiO_x and carbon nanotubes, further research and optimization are needed to achieve better performance and more extensive application. To evaluate and compare the electrochemical performance, we have tabulated the cycling stability and capacity of representative SiO_x/C composites with different carbon types mentioned above in Table 1.

5.2. Doped carbon materials

Doping carbon materials, such as graphite, in SiO_x/C composites offers several benefits. Firstly, it increases the density of defects in graphite, which reduces the energy barrier and band gap, thereby improving the electronic conductivity of the SiO_x/C composite. Additionally, carbon doping increases the electronegativity and the presence of surface-active sites on graphite, enhancing its interaction with SiO_x (Fig. 9a).[147] Han *et al.*[148] employed a high-temperature heating process to decompose organosilicon compounds within a sealed vessel. This decomposition resulted in the formation of SiOCN (SiO/N-doped carbon) microspheres. Through CVD technology, a carbon layer is grown on the surface of SiOCN in the mixed atmosphere of CH_4 and H_2. In this continuous high-temperature CVD process, with the conversion of C–H into C–C bonds through dehydrogenation reaction, the SiOCN is reduced to VG@SiO_x/NC and the N atoms come from the amino group of the organosilicon. As observed from the SEM images, VG@SiO_x/NC maintains the spherical morphology of highly round, smooth, and well-dispersed SiOCN microspheres. Moreover, the porous structure form on the surface, which not only plays a critical role of the Li^+ transport route during cycling but also improves the contact of the electrolyte with active materials. The N doping of the carbon layer can also cause the formation of large defects. These defects can increase the lithium-ion accommodation and be favourable for buffering the volume expansion of SiO_x. More importantly, the VG@SiO_x/NC fixed three-dimensional structure shows stable electrochemical performance during the charging/discharging process, which delivered a high initial reversible capacity of 1323.8 mA h g^{-1}. Hu *et al.*[149] formed a resin coating layer on the surface of SiO_x through *m*-phenylenediamine and formaldehyde by amine aldehyde condensation reaction. After high temperature annealing, SiO_x@NC with a core–shell structure is obtained. This core–shell enveloping structure can well buffer the volume change issue of SiO_x in lithium storage because the carbon layer is highly mechanically stable and highly electrically conductive. As a result, SiO_x@NC manifests a high reversible capacity with outstanding durability.

The co-doping of non-metallic atoms can significantly improve the mechanical and electrochemical properties of the carbon layer. Zhou *et al.*[89] reported a double-layer coated structure of Si particles with a B,N co-doped carbon outer layer and a SiO_x inner layer through the polymer-H_3BO_3 copyrolysis process. This structure benefits from the incorporation of polyaniline as both a carbon-network provider and a N source. Polyaniline contributes to the formation of a conductive network, enhancing the overall electrical conductivity of the composite. Additionally, the presence of boric acid enables electrostatic interactions with polyaniline, leading to the formation of a polymer network on the surface of Si particles (Fig. 9b and c). At high temperatures, with the precipitation of CO_2, H_2O and NH_3, Si@SiO_x@C-NB is obtained. Because of the synergistic effects of N and B atoms, the flexible carbon layer of Si@SiO_x@C-NB contributes to better LIB performance. The Si@SiO_x@C-NB composite revealed a charge capacity of 690 mA h g^{-1} at 5 A g^{-1} and it is obviously better than that of the single atom N-doped composite (Fig. 9d). The cyclic voltammetry peak current of different materials confirm the optimization of electronic conductivity by doping (Fig. 9e). Shi *et al.*[150] synthesized composite materials by embedding SiO_x in N,S co-doped graphene, with thiourea (CN_2H_4S) as the source of

Table 1 Electrochemical performance and carbon types of representative SiO_x/C anodes

Anode	Cycling stability (mA h g^{-1})	Rate capability (mA h g^{-1})	Carbon types	Ref.
SiO_x/G	624 after 1000 cycles at 1 A g^{-1}	661 at 10 A g^{-1}	Graphene	146
SiO_x/TiO_2@MLG	966 after 400 cycles at 2 A g^{-1}	251 at 10 A g^{-1}	Graphene	141
SiO_x@CNTs/C	1080 after 400 cycles at 0.5 A g^{-1}	284 at 10 A g^{-1}	Carbon nanotubes and graphite	18
C-SiO_x/C	234 after 200 cycles at 0.5 C	1191 at 5 C	Carbon nanotubes and graphite	15
SiO_x/MWCNTs/N-doped C	621 after 450 cycles at 0.1 A g^{-1}	388 at 800 mA g^{-1}	MWCNTs and graphite	145
NC@SiO_x@m-C	583 after 500 cycles at 1 A g^{-1}	495 at 2 A g^{-1}	Graphite	130

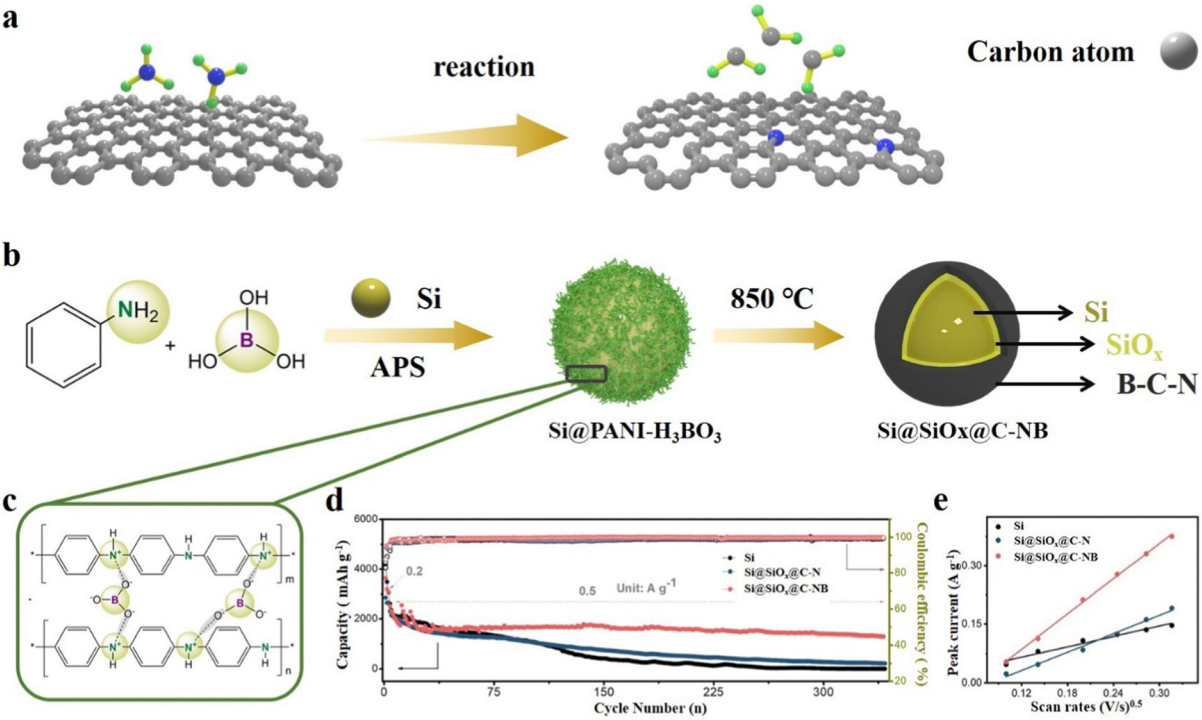

Fig. 9 (a) Schematic diagram of doping manufacturing defects. (b) Synthetic approach of Si@SiO_x@C-NB, (c) polymer molecular structure, (d) cycling stability for 340 cycles at 0.5 A g^{-1} and (e) linear fits for varying sweeping rate CV profiles.[89] Reproduced from ref. 89 with permission from John Wiley and Sons, Copyright 2022.

both N and S. Graphene oxide, SiO_x and thiourea are ultrasonically dispersed and annealed at high temperature to obtain SiO_x/N,S-rGO. The wrinkled N,S co-doped graphene can increase the specific surface area and enhance the electronic conductivity between SiO_x microparticles. Meanwhile, it may also relieve the stress and accommodate the volume changes during cycling. Zhang *et al.*[151] used rice husk as the source of both C and Si, $NH_4HB_4O_7$ as the heteroatom source and a porogen reagent to synthesize a B,N co-doped porous C/SiO_x composite by a one-step calcination strategy. With the homogeneous distribution of B and N in the porous C framework, the electronic and Li^+ conductivity can be substantially enhanced and produce abundant adsorption sites for lithium-ion storage. Due to the unique porous structure and B,N co-doping, the composite material achieves large coulomb efficiency and specific capacity. Similarly, Guo *et al.*[152] also used rice husk as the Si/C source and synthesized an Fe and N co-doped SiO_x/Fe–N–C composite by an electrospray carbonization process. Fe single atoms encapsulated in N-doped graphite frameworks improve the dispersion of SiO_x, so that the SiO_x/Fe–N–C composite shows excellent electrochemical stability. Metals can also be embedded in the SiO_x matrix, which can greatly improve the reaction kinetics of SiO_x.

5.3. Surface modification

The carbon coating improves the conductivity of the material, buffers the volume change of SiO_x, and greatly improves the cycle stability.[153] Despite its potential, the diffusion of the carbon layer to Li^+ is limited, making it challenging to form a stable SEI. This issue impedes the overall performance improvement of SiO_x/C composites. Therefore, it is a promising surface modification strategy to combine hybrid coatings with other high-performance materials.138 Coating with metal oxides has been proved to be efficient and feasible, such as Al_2O_3,[154] CeO_2,[155] MgO,[156] ZrO_2,[157,158] and TiO_2.[141,159] The surface modification of electrodes with metal oxides can reduce the direct contact between the SiO_x core and the electrolyte, and reduce the consumption of Li^+ to form a stable SEI.[160,161] Xiao *et al.*[162] synthesized SiO_x@TiO_2@C composite materials with a double-layer structure *via* an expandable experimental route. The process involves mixing SiO_x particles with titanium butoxide, followed by heating and stirring to produce SiO_x@TiO_2 precursors. CVD technology is then utilized to initiate a carbon coating reaction using propylene as the carbon source, resulting in the final product SiO_x@TiO_2@C. TiO_2 has strong mechanical stability, and the electrode material has small volume changes after lithium insertion, which can maintain the stability of the SEI. High electrochemical reversibility will not cause too many side reactions and capacity attenuation. Furthermore, the inclusion of a TiO_2 layer in the composite contributes to enhancing the overall conductivity of the material. TiO_2 possesses favourable electronic conductivity and ionic conductivity properties, allowing it to facilitate efficient charge transport within the material. This improved conductivity enables the composite to adapt to high currents, making it suitable for applications that require high-power performance.

It is hybridized with a highly graphitized carbon layer and uniformly coated on the surface of SiO_x particles, forming an efficient conductive network, greatly reducing side reactions, and significantly improving the ICE. The thermal effect of the reaction between Li_xSi and the electrolyte affects the safety of LIBs, which can lead to combustion and even explosion. The experimental results demonstrate that direct carbon coating on the surface of SiO_x@C has limited suppression of thermal effects. However, the use of SiO_x@TiO_2 significantly inhibits the generation of heat. This more stable thermal performance can be attributed to the excellent thermal stability of the lithium titanate phase. In the traditional magnesium thermal reduction reaction to generate SiO_x based negative electrode materials, HCl solution is usually used to wash away the remaining Mg and the reaction by-product MgO. Then a porous structure will be formed to alleviate the volume expansion problem. However, recent studies have found that MgO can dehydrate the electrolyte and eliminate the conditions causing HF generation, thus avoiding the corrosion of the collector and SiO_x. In a study conducted by Xu *et al.*,[155] SiO_x was obtained from SiO_2 through a process called magnesium thermal reduction. During this process, *in situ* MgO particles were incorporated into the SiO_x matrix, resulting in the formation of a SiO_x/MgO composite. Subsequently, a polymer shell was formed through phenolic condensation, encapsulating the SiO_x/MgO composite. After annealing, the composite transformed into SiO_x/MgO/Mg_2SiO_4/C. In the final composite structure, both MgO and Mg_2SiO_4 phases were uniformly distributed within the SiO_x matrix. This distribution plays a crucial role in buffering volume changes that occur during charge and discharge cycles. By buffering volume changes from all directions, the composite effectively inhibits material cracking and maintains structural integrity during cycling. In addition, the formation of Mg_2SiO_4 inhibits the formation of lithium silicate, greatly improving the initial coulomb efficiency. Cui *et al.*[163] used rice husk as a raw material to obtain the porous SiO_2/C precursor after carbonization. Then the precursor was ground with Al powder and annealed at high temperature, obtained the Al-doped porous C/SiO_2. Al_2O_3 with a suitable band gap and superior ionic conductivity can improve the rate performance of the material. Similarly, Al_2O_3, as an amphoteric oxide, can inhibit the side reaction of $LiPF_6$ based electrolyte to generate HF. Although Al_2O_3 has a negative impact on the electronic conductivity, the remaining Al nanoparticles can alleviate the influence of Al_2O_3 on conductivity. LIBs exhibit high ICE and excellent cycle stability. The metal oxide layer is relatively inert, which is not conducive to electronic conductivity. In recent years, SiO_x has also been coated with lithium salts. Kang *et al.*[164] reported a single layer LiF coated SiO_x anode material. LiF has a high Young's modulus and interface energy, which allow it to adhere well to SiO_x. During battery cycling, an inorganic-rich SEI layer is formed, which is distinct from the traditional SEI and offers superior conductivity and structural stability. Furthermore, the use of LiF in the SEI layer can enhance the thermal stability, reduce electrolyte decomposition, and improve overall battery performance. Gu *et al.*[165] designed a Li_3PO_4 coating, which can reduce the energy barrier of Li^+ transmission, and combined it with the carbon conductive framework, which greatly improved the transmission capacity of electrons and ions. In addition, Li_3PO_4 contributes to the formation of a stable SEI and the ICE is also improved.

5.4. Prelithiation

The ion conductivity and cycling performance of SiO_x based electrode materials exhibit a positive correlation with the oxygen content.[166] Pan *et al.*[167] conducted electrochemical impedance testing and constant current intermittent titration experiments and found that the diffusion rate of Li^+ was higher in SiO_x than in Si, which enabled SiO_x to charge/discharge more rapidly. After oxygen enrichment on the surface of SiO_x, a large amount of Li_xSiO_y and Li_2O will be generated during the first charge and discharge to form an SEI, resulting in irreversible consumption of Li^+ and thus reducing the ICE. In order to compensate for the loss of active lithium after the battery is assembled, prelithiation is an efficient strategy.[168] The fundamental concept behind prelithiation is to utilize an external lithium source to compensate for the lithium consumption that occurs during the initial cycle of the battery. Various prelithiation strategies exist, each requiring a distinct approach and set of materials.[169] In general, all prelithiation strategies can be divided into chemical prelithiation and electrochemical prelithiation from the reaction mechanism. Cathode prelithiation additives can be used easily, and electrochemical prelithiation is the most common for anode materials.[170]

Chemical prelithiation is realized by a chemical reaction between lithium metal or other lithium rich materials and active materials.[171] Lithium metal is the most typical anode prelithiation material because of its lowest electrochemical potential, and it can be lithiated through direct contact with electrode materials.[172] When lithium metal contacts with active substances, internal short circuit or self-discharge will occur, which will cause Li^+ to embed into the anode material and react to lithiate the anode material. In addition, this lithiation process can also form a stable SEI on the surface of the anode material, reducing the side reaction of SiO_x. Although the strategy of directly adding lithium directly improves the ICE, the addition amount of lithium metal also needs to be controlled because the excess lithium will produce dendrites during cycling, which will puncture the separators and affect the safety of the battery. Meng *et al.*[173] pressed SiO_x, the resistance buffer layer (RBL) and lithium foil together. The RBL is carbon nanotubes coated with PVB, which has high electronic and ionic conductivity. By adjusting the coating parameters of the RBL, the resistance value can be changed, thereby altering the electrode current during lithiation. Lower resistance values lead to higher currents, resulting in faster lithiation rates and greater degrees of lithiation. This simple method realizes the adjustable rate and degree of lithiation and can also make the lithiation more uniform. The treated SiO_x anode significantly improved the ICE (68% to 87%) in the full battery and could stably circulate for more than 200 cycles. In addition to direct contact with lithium metal, some lithium rich compounds can

also be added to the anode materials to achieve prelithiation, such as $Li_{2.6}Co_{0.4}N$, Li_xSi, *etc.* Zhao *et al.*[174] used SiO_x as the raw material to obtain the Li_xSi/Li_2O composite through low-cost synthesis. The Li_xSi nanodomain is uniformly embedded in the Li_2O crystal, and the ICE of this lithiated composite material is increased from 52.6% to 93.8%; even when mixed with other anode materials, the ICE can exceed 100%. In addition, irreversible Li_2O can be used as a protective layer on the surface of materials, which can maintain stable electrochemical performance even in an environment with 40% relative humidity. Although the Li_xSi alloy has low oxidation–reduction potential and high specific capacity, it can be used for prelithiation of almost all kinds of anode materials. However, Li_xSi is unstable and easily deteriorates when exposed to air, so its industrial application still faces great challenges. Solution chemical prelithiation is also an efficient and safe prelithiation strategy. The initial coulomb efficiency of Li^+ is improved by inserting the electrode material into a lithium rich organic solution for redox reaction. The reaction in solution can make the lithiation process uniform and maintain the integrity of the electrode.[175] In the research conducted by Yan *et al.*,[175] they employed a method of prelithiation by dissolving lithium tablets in a biphenyl solution of tetrahydrofuran. The SiO_x/C material was then exposed to the lithium biphenyl complex present in the composite solution. As a result of this interaction, a reaction occurred between SiO_x/C and the lithium species. This reaction led to the formation of a lithium–silicon oxide compound, denoted as Li_xSiO_y, on the surface of the SiO_x/C material. It can obviously cause lithium consumption during the first cycle and greatly improve the coulomb efficiency.

Electrochemical prelithiation is considered a viable and user-friendly approach compared to chemical prelithiation.[176] Prior to assembling the electrode material into the battery, a half cell is created using lithium metal or other lithium-containing electrode materials as the counter electrode.[177] This half cell is then charged to compensate for the lithium depletion that occurs in the negative electrode material.[178] The speed and degree of prelithiation can be precisely controlled by adjusting various parameters. Electrochemical prelithiation can form a uniform and dense SEI, but the need to assemble and disassemble the battery system increases the difficulty of large-scale application.[177] Additionally, specific charging voltage parameters for prelithiation are associated with different electrode materials. When the voltage is excessively high, full lithiation of lithium may not occur, while excessively low levels can cause the formation of observable lithium dendrites. In conclusion, multiple prelithiation methods exhibit unique characteristics. However, research on prelithiation technology remains relatively underdeveloped and immature at present.[176]

5.5. Binders

The inherent drawback of SiO_x based negative electrode materials is the expansion of volume during the cycling process. Although the use of carbon materials in composites has effectively addressed this issue, there is still potential for further improvement.[179] In order to overcome these shortcomings, a lot of research has been done to promote the industrialization of SiO_x.[180] The design of the binder also shows great potential for improving the performance of SiO_x based materials.[181] The adhesive combines the active material and the conductive agent, so the first consideration standard of the adhesive is strong interface adhesion and strong Li^+ conductivity.[182] The volume expansion of SiO_x will cause the material to crack or even pulverize, so an efficient binder should have good mechanical elasticity and strength. Elasticity can absorb the stress in the process of circulation and keeps particles in contact.[183] The development of adhesives should mainly focus on designing polymer adhesives rich in –COOH, –OH, $–NH_2$ and other polar groups.[184] The traditionally used adhesive is polyvinylidene fluoride (PVDF), but its application in SiO_x based materials cannot provide good adhesion and mitigate buffer volume change. Sodium carboxymethyl cellulose (CMC) is a commonly used adhesive due to containing a large number of hydroxyl and carboxyl groups, which enable strong adhesion to the SiO_x surface. However, during significant volume changes of SiO_x, CMC can slide and cause the material to detach or fall off. In view of this, Xue *et al.*[185] used CMC as the binder to add a small amount of Si particles as the nano-comb when making the slurry. The polar groups in the polymer can interact with the surface of Si nanoparticles to open the molecular chain of CMC. Stretched molecular chains can provide maximum adhesion and can also increase the surface contact with SiO_x to generate a uniform conductive network. Liao *et al.*[186] obtained a three-dimensional cross-linked adhesive, c-CMC-IDA_{150}, by *in situ* thermal shrinkage and reaction between iminodiacetic acid (IDA) and CMC. The crosslinking degree can be well adjusted by adjusting the mass fraction of IDA and heat treatment temperature. c-CMC-IDA_{150} has many contact sites interacting with SiO_x, which improves the surface adhesion. In addition, c-CMC-IDA_{150} can also adapt to the displacement and volume change of SiO_x particles during circulation.

The 3D network structure serves as an excellent stress buffer for SiO_x volume changes, thereby preserving the integrity of the electrode structure.[187] Furthermore, the 3D network can enhance the overall electronic conductivity of materials and facilitate the formation of stable SEI layers. The majority of binders exhibit favourable elasticity, helping to maintain the overall structure of the electrode.[188] Nevertheless, the volume of SiO_x may undergo significant changes if the elasticity of the binder is not suitable. Volume expansion extends the diffusion path of Li^+, which seriously affects the rate performance of the material. Compared with van der Waals forces and covalent bonds, hydrogen bonds have a dynamic self-healing ability and strong mechanical properties. Tang *et al.*[189] introduced tannic acid into linear polyacrylic acid, which formed a stable and reversible 3D cross-linking network structure under the action of a large number of hydrogen bonds. Hydrogen bonding can also provide SiO_x based materials with strong interfacial adhesion and cohesiveness. Compared with the CMC binder, a large number of hydrogen bonds can be dynamically broken and recombined at room temperature, resulting in excellent

electrode stability. After 50 cycles, no significant electrode cracking was observed, and 1025 mA h g^{-1} was still achievable after 250 cycles under 500 mA g^{-1}. Similarly, Weng *et al.*[190] utilized free radical polymerization of acrylamide and acrylic acid to produce covalent–noncovalent networks with exceptional elasticity. The presence of carboxyl and amide groups within the network of a material enables the formation of hydrogen bonds. These hydrogen bonds play a crucial role in enhancing the structural stability of the electrode. Furthermore, materials that are rich in hydroxyl groups (–OH) exhibit strong interactions with other components, such as binders. This strong interaction helps to mitigate binder agglomeration, which refers to the clustering or agglomeration of the binder material within the electrode.

As binders usually exhibit relatively weak conductivity, it is crucial to control the proportion of the binder. In recent years, increasing the conductivity of adhesives has also attracted extensive attention. Song *et al.*[184] designed a cross-linked conductive adhesive (CCB) with strong mechanical properties. Starting from the molecular level, it not only enhances the intrinsic electronic conductivity, but also shows good mechanical properties during electrochemical cycling through the covalent bond connection between the binders.

6. Conclusion

SiO_x (silicon oxide) is considered one of the most promising anode materials for lithium-ion batteries due to its high specific capacity. However, it is important to note that there are still challenges and issues that need to be well addressed in order to realize its full potential. The huge volume change and low electron transmission are the two key issues of SiO_x during cycling. In this review, we systematically summarize the design of SiO_x/C composite materials, focusing on their three-dimensional structure from internal and external aspects. Firstly, based on the design of the SiO_x core, the characteristics of spherical structures, nanowires and nanofilms in electrochemical performance are discussed. The hollow structure of SiO_x based anode materials offers plenty of space to accommodate the volume expansion during cycling, resulting in exceptional stress-buffering capabilities. Nanowires and nanofilms exhibit higher volume energy density, as well as an enhanced electron and ion transport ability. The oxidation degree of SiO_x is controlled by adjusting the amount of the reducing agent. A suitable oxygen content generates a more stable SEI, and excessive lithium will not be consumed during the initial cycle. The recombination with carbon has been proved through many studies to greatly improve the conductivity of SiO_x and provide a stable electrode/electrolyte interface. In addition, carbon materials have good elasticity and can buffer the volume change of SiO_x during charging. The different SiO_x/C composite structures of SiO_x/C are distinguished. The yolk@shell structure can adapt to the volume change of SiO_x well without affecting the specific mass capacity. The coating of the carbon layer can also reduce the direct contact between the electrolyte and SiO_x, and improve the stability of the SEI. On the basis of SiO_x/C, the carbon source can also be the development direction of advanced SiO_x/C composites, and the influence of carbon content on their specific capacity and cycle stability is emphasized. Furthermore, this review also summarizes various non-metallic atom doping methods that can enhance the intrinsic conductivity of the carbon coating layer. During the initial cycles, SiO_x electrodes may undergo significant side reactions, which can reduce the coulombic efficiency. To address this issue, a promising strategy is prelithiation of the electrode before cycling, thereby compensating for the lithium consumption that occurs during the first cycle. As SiO_x/C composites have better structural stability and conductivity during cycling, the choice of the binder will also determine their application. Three-dimensional crosslinked adhesives have a strong influence on mechanical and conductive properties and could be crucial for high performance Si/C Li ion batteries.

Despite ongoing research efforts to improve the electrochemical properties of high performance SiO_x based anode materials, challenges remain. For instance, to address the serious volume expansion and poor conductivity of SiO_x electrodes, researchers have developed hollow or porous SiO_x particles by the sacrificial template approach. However, this remains a challenge for industrial scale production due to the high production costs and complex processes involved. While improving the performance parameters of SiO_x in energy storage is crucial, attention must also be given to its scalability for mass production. The controlled, predictable, economical, and systematic combination of SiO_x and carbon can guide the development of advanced and practical SiO_x/C composites and electrode materials, while also providing valuable insights into other high capacity energy storage systems.

Conflicts of interest

There are no conflicts to declare.

Acknowledgements

This work was financially supported by the Key Research and Development Projects of Sichuan Province (2023YFG0222), the ''Tianfu Emei'' Science and Technology Innovation Leader Program in Sichuan Province (2021), the University of Electronic Science and Technology of China Talent Start-up Funds (A1098 5310 2360 1208), and the National Natural Science Foundation of China (21464015 and 21472235).

References

1 Z. Li, W. Tang, Y. Yang, G. Lai, Z. Lin, H. Xiao, J. Qiu, X. Wei, S. Wu and Z. Lin, *Adv. Funct. Mater.*, 2022, **32**, 220615.

2 K. Andrew, O. Seok Hyeon, A. Arindam, R. S. Bhaskar, K. Sandeep and P. Rajkumar, *J. Mater. Chem. A*, 2023, **15**, 7833–7866.
3 Z. Song, T. Zhang, L. Wang, Y. Zhao, Z. Li, M. Zhang, K. Wang, S. Xue, J. Fang, Y. Ji, F. Pan and L. Yang, *Small Methods*, 2022, **6**, 2101591.
4 Q. Li, R. Yi, Y. Xu, X. Cao, C. Wang, W. Xu and J.-G. Zhang, *J. Power Sources*, 2022, **548**, 232063.
5 R. Li, C. Fu, B. Cui, C. Cui, X. Mu, Y. Gao, G. Yin and P. Zuo, *J. Power Sources*, 2023, **554**, 232337.
6 F. Lin, J. Luo, Y. Zhang, J. Zhu, H. A. Malik, Z. Wan and C. Jia, *J. Mater. Chem. A*, 2023, **11**, 2544–2567.
7 Y. T. Malik, S.-Y. Shin, J. I. Jang, H. M. Kim, S. Cho, Y. R. Do and J.-W. Jeon, *Small*, 2022, **19**, 2206141.
8 D. Wang, C. Zhou, B. Cao, Y. Xu, D. Zhang, A. Li, J. Zhou, Z. Ma, X. Chen and H. Song, *Energy Storage Mater.*, 2020, **24**, 312–318.
9 S. E. Wang, M. J. Kim, J. W. Lee, J. Chun, J. Choi, K. C. Roh, Y. C. Kang and D. S. Jung, *Small Methods*, 2022, **6**, 2200430.
10 Q. Zhang, C. Zhang, W. Luo, L. Cui, Y.-J. Wang, T. Jian, X. Li, Q. Yan, H. Liu, C. Ouyang, Y. Chen, C.-L. Chen and J. Zhang, *Adv. Sci.*, 2020, **7**, 2200749.
11 W. Zhang, S.-B. Son, H. Guthrey and C. Ban, *Energy Storage Mater.*, 2022, **49**, 111–121.
12 W. Chen, R. V. Salvatierra, M. Ren, J. Chen, M. G. Stanford and J. M. Tour, *Adv. Mater.*, 2020, **32**, 2002850.
13 G. Ge, G. Li, X. Wang, X. Chen, L. Fu, X. Liu, E. Mao, J. Liu, X. Yang, C. Qian and Y. Sun, *Nano Lett.*, 2021, **21**, 3127–3133.
14 J. Im, J.-D. Kwon, D.-H. Kim, S. Yoon and K. Y. Cho, *Small Methods*, 2022, **6**, 2101052.
15 G. Li, L.-B. Huang, M.-Y. Yan, J.-Y. Li, K.-C. Jiang, Y.-X. Yin, S. Xin, Q. Xu and Y.-G. Guo, *Nano Energy*, 2020, **74**, 104890.
16 H. Li, H. Li, Z. Yang, L. Yang, J. Gong, Y. Liu, G. Wang, Z. Zheng, B. Zhong, Y. Song, Y. Zhong, Z. Wu and X. Guo, *Small*, 2021, **17**, 2102641.
17 Y. Li, Y. Qian, J. Zhou, N. Lin and Y. Qian, *Nano Res.*, 2022, **15**, 230–237.
18 H. Tian, H. Tian, W. Yang, F. Zhang, W. Yang, Q. Zhang, Y. Wang, J. Liu, S. R. P. Silva, H. Liu and G. Wang, *Adv. Funct. Mater.*, 2021, **31**, 2101796.
19 Y.-F. Tian, G. Li, D.-X. Xu, Z.-Y. Lu, M.-Y. Yan, J. Wan, J.-Y. Li, Q. Xu, S. Xin, R. Wen and Y.-G. Guo, *Adv. Mater.*, 2022, **34**, 2200672.
20 Y. Weng, G. Chen, F. Dou, X. Zhuang, Q. Wang, M. Lu, L. Shi and D. Zhang, *J. Energy Storage*, 2020, **32**, 101856.
21 W. Zhang, Y. Weng, W. Shen, R. Lv, F. Kang and Z.-H. Huang, *Carbon*, 2020, **158**, 163–171.
22 M. Ashuri, Q. He and L. L. Shaw, *J. Power Sources*, 2023, **559**, 232660.
23 H. Li, S. Zhu, S. Li, Q. Zhang, J. Zhao and L. Zhang, *Chem. J. Chin. Univ.*, 2021, **42**, 2342–2358.
24 H. R. Philipp, *J. Phys. Chem. Solids*, 1971, **32**, 1935–1945.
25 H. R. Philipp, *J. Non-Cryst. Solids*, 1972, **8–10**, 627–632.
26 R. J. Temkin, *J. Non-Cryst. Solids*, 1975, **17**, 215–230.
27 A. Hohl, T. Wieder, P. A. van Aken, T. E. Weirich, G. Denninger, M. Vidal, S. Oswald, C. Deneke, J. Mayer and H. Fuess, *J. Non-Cryst. Solids*, 2003, **320**, 255–280.
28 E. Fuglein and U. Schubert, *Chem. Mater.*, 1999, **11**, 865–866.
29 A. Hirata, S. Kohara, T. Asada, M. Arao, C. Yogi, H. Imai, Y. Tan, T. Fujita and M. Chen, *Nat. Commun.*, 2016, **7**, 1–7.
30 R. Wang, H. Li, Y. Wu, H. Li, B. Zhong, Y. Sun, Z. Wu and X. Guo, *Adv. Energy Mater.*, 2022, **12**, 2202342.
31 A. Su, J. Li, J. Dong, D. Yang, G. Chen and Y. Wei, *Small*, 2020, **16**, 2001714.
32 S. Bazlen, P. Heugel, O. von Kessel, W. Commerell and J. Tuebke, *J. Energy Storage*, 2022, **49**, 104044.
33 H. P. Boehm, R. Setton and E. Stumpp, *Pure Appl. Chem.*, 1994, **66**, 1893–1901.
34 T. Yao, N. Ozawa, T. Aikawa and S. Yoshinaga, *Solid State Ionics*, 2004, **175**, 199–202.
35 H. Wu, L. Zheng, J. Zhan, N. Du, W. Liu, J. Ma, L. Su and L. Wang, *J. Power Sources*, 2020, **449**, 227513.
36 Z. Ma, A. Song, Z. Liu, Y. Guo, X. Yang, Q. Li, Y. Fan, L. Dai, H. Tian, X. Qin, H. Liu, G. Shao and G. Wang, *Adv. Funct. Mater.*, 2023, **33**, 2301112.
37 H. Wu, L. Zheng, N. Du, B. Sun, J. Ma, Y. Jiang, J. Gong, H. Chen and L. Wang, *ACS Appl. Mater. Interfaces*, 2021, **13**, 22323–22331.
38 N. Yao, Y. Zhang, X. Rao, Z. Yang, K. Zheng, K. Swierczek and H. Zhao, *Int. J. Miner., Metall. Mater.*, 2022, **29**, 876–895.
39 X. Zhu, B. Liu, J. Shao, Q. Zhang, Y. Wan, C. Zhong and J. Lu, *Adv. Funct. Mater.*, 2023, **33**, 2213363.
40 S. Zhu, H. Li, Z. Hu, Q. Zhang, J. Zhao and L. Zhang, *Acta Phys.-Chim. Sin.*, 2022, **38**, 628233.
41 X. Zhou, Z. Qi, Q. Liu, J. Tian, M. Liu, K. Dong and Z. Lei, *Front. Mater.*, 2021, **7**, 628233.
42 G. Zhu, D. Chao, W. Xu, M. Wu and H. Zhang, *ACS Nano*, 2021, **15**, 15567–15593.
43 X. Zhang, H. Shi, P. Lv, J. Liu and H. Zhang, *Energy Technol.*, 2021, **9**, 2100400.
44 M. Li, C. Ye, Z. Li, Q. Lin, J. Cao, F. Liu, G. Song and S. Kawi, *J. Mater. Chem. A*, 2022, **10**, 6330–6350.
45 J. Tao, Z. Yan, J. Yang, J. Li, Y. Lin and Z. Huang, *Carbon Energy*, 2022, **4**, 129–141.
46 Q. Hua, D. Dai, C. Zhang, F. Han, T. Lv, X. Li, S. Wang, R. Zhu, H. Liao and S. Zhang, *Nanoscale Res. Lett.*, 2018, **13**, 134–139.
47 Y. Cao, J. C. Bennett, R. A. Dunlap and M. N. Obrovac, *Chem. Mater.*, 2018, **30**, 7418–7422.
48 P. Zhang, L. Wang, J. Xie, L. Su and C.-A. Ma, *J. Mater. Chem. A*, 2014, **2**, 3776–3782.
49 H.-S. Kim, W. Cho, D. Park, K. Kim, W.-S. Jung, H. Choi and J.-H. Kim, *J. Alloys Compd.*, 2019, **803**, 325–331.
50 K. Zeng, T. Li, X. Qin, G. Liang, L. Zhang, Q. Liu, B. Li and F. Kang, *Nano Res.*, 2020, **13**, 2987–2993.
51 K. Wang, Y. Tan, P. Li and J. Sun, *Electrochim. Acta*, 2020, **353**, 136538.
52 A. Raza, J. Y. Jung, C.-H. Lee, B. G. Kim, J.-H. Choi, M.-S. Park and S.-M. Lee, *ACS Appl. Mater. Interfaces*, 2021, **13**, 7161–7170.

53 T. Wu, Q. Ke, M. Lu, P. Pan, Y. Zhou, Z. Gu, G. Cui and H. Lu, *Catalysts*, 2022, **12**, 2–28.
54 X. Zhou, Y. Liu, Y. Ren, T. Mu, X. Yin, C. Du, H. Huo, X. Cheng, P. Zuo and G. Yin, *Adv. Funct. Mater.*, 2021, **31**, 2101145.
55 T. Xu, Q. Wang, J. Zhang, X. Xie and B. Xia, *ACS Appl. Mater. Interfaces*, 2019, **11**, 19959–19967.
56 C. Guo, Y. Xie, K. Pan and L. Li, *Nanoscale*, 2020, **12**, 13017–13027.
57 O. J. Sanumi, P. G. Ndungu and B. O. Oboirien, *J. Power Sources*, 2022, **543**, 231849.
58 A. Staerz, H. G. Seo, T. Defferriere and H. L. Tuller, *J. Mater. Chem. A*, 2022, **10**, 2618–2636.
59 V. Pavlenko, S. Khosravi, S. Zoltowska, A. B. Haruna, M. Zahid, Z. Mansurov, Z. Supiyeva, A. Galal, K. I. Ozoemena, Q. Abbas and T. Jesionowski, *Mater. Sci. Eng., R*, 2022, **149**, 100682.
60 Z. Li, Q. He, L. He, P. Hu, W. Li, H. Yan, X. Peng, C. Huang and L. Mai, *J. Mater. Chem. A*, 2017, **5**, 4183–4189.
61 A. Kim, S. Lim, D.-H. Peck, S.-K. Kim, B. Lee and D. Jung, *Nanomaterials*, 2012, **2**, 206–216.
62 Z. Wang, L. Kong, Z. Guo, X. Zhang, X. Wang and X. Zhang, *Chem. Eng. J.*, 2022, **428**, 131060.
63 Q. Liu, Z. Cui, R. Zou, J. Zhang, K. Xu and J. Hu, *Small*, 2017, **13**, 1603754.
64 M. Chen, X. Ma, B. Chen, R. Arsenault, P. Karlson, N. Simon and Y. Wang, *Joule*, 2019, **3**, 2622–2646.
65 H. Takezawa, S. Ito, H. Yoshizawa and T. Abe, *J. Power Sources*, 2016, **324**, 45–51.
66 L. F. Castaneda, J. F. Rodriguez and J. L. Nava, *Chem. Eng. J.*, 2021, **413**, 127529.
67 L. Su, J. Xie, Y. Xu, L. Wang, Y. Wang and M. Ren, *J. Alloys Compd.*, 2016, **663**, 524–530.
68 J. Yang, Y. Takeda, N. Imanishi, C. Capiglia, J. Y. Xie and O. Yamamoto, *Solid State Ionics*, 2002, **152–153**, 125–129.
69 J. Moon, *Int. J. Energy Res.*, 2021, **45**, 7315–7325.
70 J. H. Cho, X. Xiao, M. W. Verbrugge and B. W. Sheldon, *ACS Appl. Energy Mater.*, 2022, **5**, 13293–13306.
71 J. Ge, H. Shen, F. Zhou, Y. Li, N. Yuan, W. Yang, H. Zhou, B. Xu, R. Guo and P. Xu, *J. Mater. Chem. A*, 2022, **10**, 1928–1939.
72 S. Fan, X. Zhou, J. Tang, Y. Ma and J. Yang, *Appl. Surf. Sci.*, 2022, **579**, 152179.
73 J. Chai, N. Han, S. Feng, X. Huang, B. Tang and W. Zhang, *Chem. Eng. J.*, 2023, **453**, 139768.
74 S. Chae, S.-H. Choi, N. Kim, J. Sung and J. Cho, *Angew. Chem., Int. Ed.*, 2020, **59**, 110–135.
75 P. Li, H. Kim, S.-T. Myung and Y.-K. Sun, *Energy Storage Mater.*, 2021, **35**, 550–576.
76 J. Gao, C. Chen, Q. Dong, J. Dai, Y. Yao, T. Li, A. Rundlett, R. Wang, C. Wang and L. Hu, *Adv. Mater.*, 2021, **33**, 2005305.
77 J. Sung, J. Ma, S. H. Choi, J. Hong, N. Kim, S. Chae, Y. Son, S. Y. Kim and J. Cho, *Adv. Mater.*, 2019, **33**, 1900970.
78 H. Gu, Y. Wang, Y. Zeng, M. Yu, T. Liu, J. Chen, K. Wang, J. Xie and L. Li, *ACS Appl. Mater. Interfaces*, 2022, **14**, 17388–17395.
79 Z. Cao, X. Zheng, Q. Qu, Y. Huang and H. Zheng, *Adv. Mater.*, 2021, **33**, 2103178.
80 J. Zhang, X. Zhang, C. Zhang, Z. Liu, J. Zheng, Y. Zuo, C. Xue, C. Li and B. Cheng, *Energy Fuels*, 2017, **31**, 8758–8763.
81 L. Lee, W. To, A. Ran, J.-H. Lee, S. M. Hwang and Y.-J. Kim, *Chem. Eng. J.*, 2022, **442**, 136166.
82 J. Zhang, P. Ma, X. Zhang, Z. Liu, J. Zheng, Y. Zuo, C. Xue, B. Cheng and C. Li, *Energy Technol.*, 2019, **7**, 1800800.
83 L. Shi, W. Wang, A. Wang, K. Yuan, Z. Jin and Y. Yang, *J. Power Sources*, 2016, **318**, 184–191.
84 P. Lv, H. Zhao, C. Gao, T. Zhang and X. Liu, *Electrochim. Acta*, 2015, **152**, 345–351.
85 B. Liang, Y. Liu and Y. Xu, *J. Power Sources*, 2014, **267**, 469–490.
86 H. Li, J. Peng, Z. Wu, X. Liu, P. Liu, B. Chang and X. Wang, *Chem. Eng. J.*, 2023, **462**, 142172.
87 Z. Wang, H. Zhang, X. Zhang, X. Wang and X. Zhang, *Composites, Part B*, 2022, **247**, 110308.
88 J. Guo, G. Zhao, T. Xie, D. Dong, C. Ma, L. Su, L. Gong, X. Lou, X. Guo, J. Wang and Y. Zhu, *ACS Appl. Mater. Interfaces*, 2020, **12**, 19023–19032.
89 J. Zhou, Y. Lu, L. Yang, W. Zhu, W. Liu, Y. Yang and K. Liu, *Carbon Energy*, 2022, **4**, 399–410.
90 G. Zhu, Y. Gu, S. Heng, Y. Wang, Q. Qu and H. Zheng, *Electrochim. Acta*, 2019, **323**, 134840.
91 H. Zhang, K. Liu, Y. Liu, Z. Lang, W. He, L. Ma, J. Man, G. Jia, J. Cui and J. Sun, *J. Power Sources*, 2020, **447**, 227400.
92 J. Cui, Y. Cui, S. Li, H. Sun, Z. Wen and J. Sun, *ACS Appl. Mater. Interfaces*, 2016, **8**, 30239–30247.
93 Y.-F. Tian, G. Li, D.-X. Xu, Z.-Y. Lu, M.-Y. Yan, J. Wan, J.-Y. Li, Q. Xu, S. Xin, R. Wen and Y.-G. Guo, *Adv. Mater.*, 2022, **34**, 2200672.
94 P. Li, G. Zhao, X. Zheng, X. Xu, C. Yao, W. Sun and S. X. Dou, *Energy Storage Mater.*, 2018, **15**, 422–446.
95 H. Tian, F. Huang, Y. Zhu, S. Liu, Y. Han, M. Jaroniec, Q. Yang, H. Liu, G. Q. M. Lu and J. Liu, *Adv. Funct. Mater.*, 2018, **28**, 1801737.
96 Q. Shi, J. Zhou, S. Ullah, X. Yang, K. Tokarska, B. Trzebicka, H. Q. Ta and M. H. Ruemmeli, *Energy Storage Mater.*, 2021, **34**, 735–754.
97 N. Liu, H. Wu, M. T. McDowell, Y. Yao, C. Wang and Y. Cui, *Nano Lett.*, 2012, **12**, 3315–3321.
98 Z. Liu, Y. Zhao, R. He, W. Luo, J. Meng, Q. Yu, D. Zhao, L. Zhou and L. Mai, *Energy Storage Mater.*, 2019, **19**, 299–305.
99 Q. Wang, M. Zhu, G. Chen, N. Dudko, Y. Li, H. Liu, L. Shi, G. Wu and D. Zhang, *Adv. Mater.*, 2022, **34**, 2109658.
100 Q. Man, Y. An, C. Liu, H. Shen, S. Xiong and J. Feng, *J. Energy Chem.*, 2023, **76**, 576–600.
101 P. Ares and K. S. Novoselov, *Nano Mater. Sci.*, 2022, **4**, 3–9.
102 H. Luo, X. Zhang, C. Xu, W. He, Z. Wang, W. Cai and Y. Zhang, *ACS Appl. Energy Mater.*, 2022, **5**, 8982–8989.
103 H. Wang, X. Que, Y. Liu, X. Wu, Q. Yuan, J. Lu and W. Gan, *J. Alloys Compd.*, 2021, **874**, 159913.
104 M. Ku, D. Park, M. Kim, M. Choi and W. Choi, *J. Mater. Chem. A*, 2023, **11**, 15277–15285.

105 Y. Zhang, G. Hu, Q. Yu, Z. Liu, C. Yu, L. Wu, L. Zhou and L. Mai, *Mater. Chem. Front.*, 2020, **4**, 1656–1663.
106 W. Chen, S. Kuang, H. Wei, P. Wu, T. Tang, H. Li, Y. Liang, X. Yu and J. Yu, *J. Colloid Interface Sci.*, 2022, **610**, 583–591.
107 Q. Gong, H. Wang, W. Song, B. Sun, P. Cao, S. Gu, X. Sun and G. Zhou, *Chem. – Eur. J.*, 2021, **27**, 2654–2661.
108 H. Tian, H. Tian, S. Wang, S. Chen, F. Zhang, L. Song, H. Liu, J. Liu and G. Wang, *Nat. Commun.*, 2020, **11**, 5025.
109 D. Wang, T. Wang, M. He, T. Wang and H. Wang, *Small*, 2021, **17**, 2103673.
110 T. Liu, Y. Qu, J. Liu, L. Zhang, B. Cheng and J. Yu, *Small*, 2021, **17**, 14903–14909.
111 H. Wang, C.-J. Yao, H.-J. Nie, K.-Z. Wang, Y.-W. Zhong, P. Chen, S. Mei and Q. Zhang, *J. Mater. Chem. A*, 2020, **8**, 11906–11922.
112 Q. Yu, P. Ge, Z. Liu, M. Xu, W. Yang, L. Zhou, D. Zhao and L. Mai, *J. Mater. Chem. A*, 2018, **6**, 14903–14909.
113 S. Sim, P. Oh, S. Park and J. Cho, *Adv. Mater.*, 2013, **25**, 4498–4503.
114 K. Xiao, Q. Yin, X. Wu and C. Huang, *Nano Mater. Sci.*, 2022, **4**, 383–392.
115 C. Duan, K. Liang, Z. Zhang, J. Li, T. Chen, D. Lv, L. Li, L. Kang, K. Wang, H. Hu and H. Xi, *Nano Mater. Sci.*, 2022, **4**, 351–365.
116 L. Zhang, J. Deng, L. Liu, W. Si, S. Oswald, L. Xi, M. Kundu, G. Ma, T. Gemming, S. Baunack, F. Ding, C. Yan and O. G. Schmidt, *Adv. Mater.*, 2014, **26**, 4527–4532.
117 Q. Xu, J.-K. Sun, Y.-X. Yin and Y.-G. Guo, *Adv. Funct. Mater.*, 2018, **28**, 1705235.
118 S. Park, J. Sung, S. Chae, J. Hong, T. Lee, Y. Lee, H. Cha, S. Y. Kim and J. Cho, *ACS Nano*, 2020, **14**, 11548–11557.
119 H. Xue, Y. Cheng, Q. Gu, Z. Wang, Y. Shen, D. Yin, L. Wang and G. Huang, *Nanoscale*, 2021, **13**, 3808–3816.
120 Z. Wang, L. Kong, Z. Guo, X. Zhang, X. Wang and X. Zhang, *Chem. Eng. J.*, 2022, **428**, 131060.
121 S. Li, K. Wang, G. Zhang, S. Li, Y. Xu, X. Zhang, X. Zhang, S. Zheng, X. Sun and Y. Ma, *Adv. Funct. Mater.*, 2022, **32**, 2200796.
122 W.-H. Li, Y.-M. Li, X.-F. Liu, Z.-Y. Gu, H.-J. Liang, X.-X. Zhao, J.-Z. Guo and X.-L. Wu, *Adv. Funct. Mater.*, 2022, **32**, 2201038.
123 H.-J. Liang, Z.-Y. Gu, X.-X. Zhao, J.-Z. Guo, J.-L. Yang, W.-H. Li, B. Li, Z.-M. Liu, Z.-H. Sun, J.-P. Zhang and X.-L. Wu, *Sci. Bull.*, 2022, **67**, 1581–1588.
124 Q. Liu, R. Xu, D. Mu, G. Tan, H. Gao, N. Li, R. Chen and F. Wu, *Carbon Energy*, 2022, **4**, 458–479.
125 H. Tian, J. Liang and J. Liu, *Adv. Mater.*, 2019, **31**, 1903886.
126 X. Min, G. Xu, B. Xie, P. Guan, M. Sun and G. Cui, *Energy Storage Mater.*, 2022, **47**, 297–318.
127 M. Peng, K. Shin, L. Jiang, Y. Jin, K. Zeng, X. Zhou and Y. Tang, *Angew. Chem., Int. Ed.*, 2022, **61**, e202206770.
128 J. Scharf, M. Chouchane, D. P. Finegan, B. Lu, C. Redquest, M.-C. Kim, W. Yao, A. A. Franco, D. Gostovic, Z. Liu, M. Riccio, F. Zelenka, J.-M. Doux and Y. S. Meng, *Nat. Nanotechnol.*, 2022, **17**, 446–459.
129 H. Li, H. Li, Y. Lai, Z. Yang, Q. Yang, Y. Liu, Z. Zheng, Y. Liu, Y. Sun, B. Zhong, Z. Wu and X. Guo, *Adv. Energy Mater.*, 2022, **12**, 2102181.
130 Q. Ouyang, G. Li, X. Zhang, X. Zhao, Y. Wang, Q. Wang, Z. Fan, J. Wang and L. Li, *Chem. Eng. J.*, 2023, **460**, 141762.
131 G. Hu, R. Yu, Z. Liu, Q. Yu, Y. Zhang, Q. Chen, J. Wu, L. Zhou and L. Mai, *ACS Appl. Mater. Interfaces*, 2021, **13**, 3991–3998.
132 R. F. H. Hernandha, P. C. Rath, B. Umesh, J. Patra, C.-Y. Huang, W.-W. Wu, Q.-F. Dong, J. Li and J.-K. Chang, *Adv. Funct. Mater.*, 2021, **31**, 2104135.
133 Q. Sun, J. Li, M. Yang, S. Wang, G. Zeng, H. Liu, J. Cheng, D. Li, Y. Wei, P. Si, Y. Tian and L. Ci, *Small*, 2023, **19**, 2300759.
134 L. Sun, Y. Liu, R. Shao, J. Wu, R. Jiang and Z. Jin, *Energy Storage Mater.*, 2022, **46**, 482–502.
135 W. Chen, H. Liu, S. Kuang, H. Huang, T. Tang, M. Zheng, Y. Fang and X. Yu, *Carbon*, 2021, **179**, 377–386.
136 W. Chen, D. Xu, S. Kuang, Z. Wu, H. Hu, M. Zheng and X. Yu, *J. Power Sources*, 2021, **489**, 229459.
137 X. Guo, Y.-Z. Zhang, F. Zhang, Q. Li, D. H. Anjum, H. Liang, Y. Liu, C.-S. Liu, H. N. Alshareef and H. Pang, *J. Mater. Chem. A*, 2019, **7**, 15969–15974.
138 T. Meng, B. Li, C. Liu, Q. Wang, D. Shu, S. Ou, M. S. Balogun, H. Su and Y. Tong, *Energy Storage Mater.*, 2022, **46**, 344–351.
139 J. A. Buledi, N. Mahar, A. Mallah, A. R. Solangi, I. M. Palabiyik, N. Qambrani, F. Karimi, Y. Vasseghian and H. Karimi-Maleh, *Food Chem. Toxicol.*, 2022, **161**, 112843.
140 Y. Mu, M. Han, B. Wu, Y. Wang, Z. Li, J. Li, Z. Li, S. Wang, J. Wan and L. Zeng, *Adv. Sci.*, 2022, **9**, 2104685.
141 H. Xue, Y. Wu, Y. Zou, Y. Shen, G. Liu, Q. Li, D. Yin, L. Wang and J. Ming, *Adv. Funct. Mater.*, 2020, **30**, 1910657.
142 L. Lee, W. T. A. Ran, J.-H. Lee, S. M. Hwang and Y. J. Kim, *Chem. Eng. J.*, 2022, **442**, 136166.
143 J. Dai, H. Feng, K. Shi, X. Ma, Y. Yan, L. Ye and Y. Xia, *Chemosphere*, 2022, **307**, 135833.
144 T. H. Nguyen, D. Yang, B. Zhu, H. Lin, T. Ma and B. Jia, *J. Mater. Chem. A*, 2021, **9**, 7366–7395.
145 Y. Ren, X. Wu and M. Li, *Electrochim. Acta*, 2016, **206**, 328–336.
146 Q. Xu, J.-K. Sun, Z.-L. Yu, Y.-X. Yin, S. Xin, S.-H. Yu and Y.-G. Guo, *Adv. Mater.*, 2018, **30**, 1707430.
147 X. Yue, S. Huang, J. Cai, Y. Jin and P. K. Shen, *J. Mater. Chem. A*, 2017, **5**, 7784–7790.
148 M. Han, Y. Mu, F. Yuan, J. Liang, T. Jiang, X. Bai and J. Yu, *J. Mater. Chem. A*, 2020, **8**, 3822–3833.
149 G. Hu, K. Zhong, R. Yu, Z. Liu, Y. Zhang, J. Wu, L. Zhou and L. Mai, *J. Mater. Chem. A*, 2020, **8**, 13285–13291.
150 L. Shi, Y. Li, Y. Xing, R. Lin, G. Cheng, J. Ding and K. H. Lam, *Electrochim. Acta*, 2021, **390**, 138841.
151 H. Zhang, Y. Du, N. Zhang, P. Lin, W. Liu, Z. Wen, J. Cui and J. Sun, *Microporous Mesoporous Mater.*, 2022, **335**, 111794.
152 X. Guo, H. Xu, W. Li, Y. Liu, Y. Shi, Q. Li and H. Pang, *Adv. Sci.*, 2022, **10**, 2206084.

153 D. Cao, X. Sun, Y. Li, A. Anderson, W. Lu and H. Zhu, *Adv. Mater.*, 2022, **34**, 2200401.
154 Q.-H. Wu, B. Qu, J. Tang, C. Wang, D. Wang, Y. Li and J.-G. Ren, *Electrochim. Acta*, 2015, **156**, 147–153.
155 H.-W. Ha, K. H. Jeong, N. J. Yun, M. Z. Hong and K. Kim, *Electrochim. Acta*, 2005, **50**, 3764–3769.
156 Z. Wang, C. Wu, L. Liu, F. Wu, L. Chen and X. Huang, *J. Electrochem. Soc.*, 2002, **149**, A466–A471.
157 J. Cho, H. Kim and B. Park, *J. Electrochem. Soc.*, 2004, **151**, A1707–A1711.
158 Y.-M. Lin, H.-C. Wu, Y.-C. Yen, Z.-Z. Guo, M.-H. Yang, H.-M. Chen, H.-S. Sheu and N.-L. Wu, *J. Electrochem. Soc.*, 2005, **152**, A1526–A1532.
159 Y. Jiang, S. Liu, Y. Ding, J. Jiang, W. Li, S. Huang, Z. Chen, B. Zhao and J. Zhang, *J. Power Sources*, 2020, **467**, 228301.
160 T. Tao, S. Lu, Y. Fan, W. Lei, S. Huang and Y. Chen, *Adv. Mater.*, 2017, **29**, 1700542.
161 H. Tian, A. Song, H. Tian, J. Liu, G. Shao, H. Liu and G. Wang, *Chem. Sci.*, 2021, **12**, 7656–7676.
162 Z. Xiao, C. Yu, X. Lin, X. Chen, C. Zhang, H. Jiang, R. Zhang and F. Wei, *Nano Energy*, 2020, **77**, 104890.
163 J. Cui, J. Yang, J. Man, S. Li, J. Yin, L. Ma, W. He, J. Sun and J. Hu, *Electrochim. Acta*, 2019, **300**, 470–481.
164 T. Kang, J. Tan, X. Li, J. Liang, H. Wang, D. Shen, Y. Wu, Z. Huang, Y. Lu, Z. Tong and C.-S. Lee, *J. Mater. Chem. A*, 2021, **9**, 7807–7816.
165 L. Gu, J. Han, M. Chen, W. Zhou, X. Wang, M. Xu, H. Lin, H. Liu, H. Chen, J. Chen, Q. Zhang and X. Han, *Energy Storage Mater.*, 2022, **52**, 547–561.
166 X.-Y. Yue, Y.-X. Yao, J. Zhang, S.-Y. Yang, Z. Li, C. Yan and Q. Zhang, *Adv. Mater.*, 2022, **34**, 2110337.
167 S. Pan, L. Yang, P. Su, H. Zhang and S. Zhang, *Small*, 2022, **18**, 2202137.
168 B. H. Park, G.-W. Lee, S. B. Choi, Y.-H. Kim and K. B. Kim, *Nanoscale*, 2020, **12**, 22140–22149.
169 X. Song, Y. Lu, C. Li, F. Wang and X. Zhao, *J. Energy Storage*, 2022, **51**, 104390.
170 Y. Shen, X. Shen, M. Yang, J. Qian, Y. Cao, H. Yang, Y. Luo and X. Ai, *Adv. Funct. Mater.*, 2021, **31**, 2101181.
171 Y. Huang, C. Liu, F. Wei, G. Wang, L. Xiao, J. Lu and L. Zhuang, *J. Mater. Chem. A*, 2020, **8**, 18715–18720.
172 Y. Xue, J. Deng, C. Wang, R. G. Mendes, L. Chen, Y. Xiao, Q. Zhang, T. Zhang, X. Hu, X. Li, M. H. Rümmeli and L. Fu, *J. Mater. Chem. A*, 2016, **4**, 5395–5401.
173 Q. Meng, G. Li, J. Yue, Q. Xu, Y.-X. Yin and Y.-G. Guo, *ACS Appl. Mater. Interfaces*, 2019, **11**, 32062–32068.
174 J. Zhao, H.-W. Lee, J. Sun, K. Yan, Y. Liu, W. Liu, Z. Lu, D. Lin, G. Zhou and Y. Cui, *Proc. Natl. Acad. Sci. U. S. A.*, 2016, **113**, 7408–7413.
175 M.-Y. Yan, G. Li, J. Zhang, Y.-F. Tian, Y.-X. Yin, C.-J. Zhang, K.-C. Jiang, Q. Xu, H.-L. Li and Y.-G. Guo, *ACS Appl. Mater. Interfaces*, 2020, **12**, 27202–27209.
176 K. Zou, W. Deng, P. Cai, X. Deng, B. Wang, C. Liu, J. Li, H. Hou, G. Zou and X. Ji, *Adv. Funct. Mater.*, 2020, **31**, 2005581.
177 M. Fan, Q. Meng, X. Chang, C. F. Gu, X. H. Meng, Y. X. Yin, H. Li, L. J. Wan and Y. G. Guo, *Adv. Energy Mater.*, 2022, **12**, 2103630.
178 Z. Jingxi, C. Xi, S. Gang, W. Hailong, D. Yanhao and W. Chang-An, *J. Mater. Chem. A*, 2023, **11**, 8757–8765.
179 W. Wu, Y. Kang, M. Wang, D. Xu, J. Wang, Y. Cao, C. Wang and Y. Deng, *J. Power Sources*, 2020, **464**, 228224.
180 W. Kunther, S. Ferreiro and J. Skibsted, *J. Mater. Chem. A*, 2017, **11**, 8757–8765.
181 T. Meng, B. Li, Q. Wang, J. Hao, B. Huang, F. L. Gu, H. Xu, P. Liu and Y. Tong, *ACS Nano*, 2020, **14**, 7066–7076.
182 Z. Wang, X. Xu, C. Chen, T. Huang and A. Yu, *J. Power Sources*, 2022, **539**, 231604.
183 X. Sun, L. Geng, S. Yi, C. Li, Y. An, X. Zhang, X. Zhang, K. Wang and Y. Ma, *J. Power Sources*, 2021, **499**, 229936.
184 Z. Song, S. Chen, Y. Zhao, S. Xue, G. Qian, J. Fang, T. Zhang, C. Long, L. Yang and F. Pan, *Small*, 2021, **17**, 2102256.
185 S. Xue, Y. Fu, Z. Song, S. Chen, Y. Ji, Y. Zhao, H. Wang, G. Qian, L. Yang and F. Pan, *Energy Environ. Mater.*, 2022, **5**, 1310–1316.
186 H. Liao, W. He, N. Liu, D. Luo, H. Dou and X. Zhang, *ACS Appl. Mater. Interfaces*, 2021, **13**, 49313–49321.
187 A. N. Preman, H. Lee, J. Yoo, I. T. Kim, T. Saito and S.-K. Ahn, *J. Mater. Chem. A*, 2020, **8**, 25548–25570.
188 Z. Shi, Q. Liu, Z. Yang, L. A. Robertson, S. R. Bheemireddy, Y. Zhao, Z. Zhang and L. Zhang, *J. Mater. Chem. A*, 2021, **10**, 1380–1389.
189 W. Tang, L. Feng, X. Wei, G. Lai, H. Chen, Z. Li, X. Huang, S. Wu and Z. Lin, *ACS Appl. Mater. Interfaces*, 2022, **14**, 56910–56918.
190 Z. Weng, S. Di, L. Chen, G. Wu, Y. Zhang, C. Jia, N. Zhang, X. Liu and G. Chen, *ACS Appl. Mater. Interfaces*, 2022, **14**, 42494–42503.